

# CORALIE radial-velocity search for companions around evolved stars (CASCADES)

## I. Sample definition and first results: Three new planets orbiting giant stars <sup>★,★★</sup>

G. Ottoni<sup>1</sup>, S. Udry<sup>1</sup>, D. Ségransan<sup>1</sup>, G. Buldgen<sup>1</sup>, C. Lovis<sup>1</sup>, P. Eggenberger<sup>1</sup>, C. Pezzotti<sup>1</sup>, V. Adibekyan<sup>2,3</sup>,  
M. Marmier<sup>1</sup>, M. Mayor<sup>1</sup>, N.C. Santos<sup>2,3</sup>, S.G. Sousa<sup>2</sup>, N. Lagarde<sup>4</sup>, and C. Charbonnel<sup>1</sup>

<sup>1</sup> Département d'Astronomie, Université de Genève, Chemin Pegasi 51, 1290 Versoix, Switzerland. e-mail: gael.ottoni@unige.ch

<sup>2</sup> Instituto de Astrofísica e Ciências do Espaço, Universidade do Porto, CAUP, Rua das Estrelas, 4150-762 Porto, Portugal

<sup>3</sup> Departamento de Física e Astronomia, Faculdade de Ciências, Universidade do Porto, Rua do Campo Alegre, 4169-007 Porto, Portugal

<sup>4</sup> Institut UTINAM, CNRS UMR 6213, Université Bourgogne Franche-Comté, OSU THETA Franche-Comté-Bourgogne, Observatoire de Besançon, BP 1615, 25010, Besançon Cedex, France

Received December 7th, 2020; accepted November 29th 2021

### ABSTRACT

*Context.* Following the first discovery of a planet orbiting a giant star in 2002, we started the CORALIE radial-velocity search for companions around evolved stars (CASCADES). We present the observations of three stars conducted at the 1.2 m Leonard Euler Swiss telescope at La Silla Observatory, Chile, using the CORALIE spectrograph.

*Aims.* We aim to detect planetary companions to intermediate-mass G- and K- type evolved stars and perform a statistical analysis of this population. We searched for new planetary systems around the stars HD 22532 (TIC 200851704), HD 64121 (TIC 264770836), and HD 69123 (TIC 146264536).

*Methods.* We have followed a volume-limited sample of 641 red giants since 2006 to obtain high-precision radial-velocity measurements. We used the Data & Analysis Center for Exoplanets (DACE) platform to perform a radial-velocity analysis to search for periodic signals in the line profile and activity indices, to distinguish between planetary-induced radial-velocity variations and stellar photospheric jitter, and to search for significant signals in the radial-velocity time series to fit a corresponding Keplerian model.

*Results.* In this paper, we present the survey in detail, and we report on the discovery of the first three planets of the sample around the giant stars HD 22532, HD 64121, and HD 69123.

**Key words.** Techniques: radial velocities – Planets and satellites: detection – (Stars:) planetary systems – Stars: individual – HD 22532, HD 64121, HD 69123, TIC 200851704, TIC 264770836, TIC 146264536

## 1. Introduction

Since the discovery of 51 Peg b by Mayor & Queloz (1995), the first extrasolar planet orbiting a solar-like star, over 4800 exoplanets<sup>1</sup> have been detected, including almost 900 using the radial-velocity technique. Those distant worlds cover a broad diversity of orbital properties (Udry & Santos 2007; Winn & Fabrycky 2014), expected to be fossil traces of the formation process of these systems and potentially linked as well to the properties and evolutionary stages of their host stars and their environments.

Models of planetary formation were at first developed based on the system we know best, the Solar System, and have evolved significantly in the past twenty years with the increasing flow of information derived from observations of exoplanet systems. The observed diversity of planet properties finds its origin in

\* Based on observations collected with the CORALIE echelle spectrograph on the 1.2-m Euler Swiss telescope at La Silla Observatory, ESO, Chile.

\*\* The complete Table 2 is only available in electronic form at the CDS via anonymous ftp to [cdsarc.u-strasbg.fr/](https://cdsarc.u-strasbg.fr/) (130.79.128.5) or via CDS

<sup>1</sup> See e.g., <https://exoplanetarchive.ipac.caltech.edu> (as of January 5, 2022).

the physical process at play coupled with the local conditions during the formation of the system. Today, two main competing paradigms are proposed for planet formation: the core accretion model: a dust-to-planet bottom-up scenario (e.g., Lissauer 1993; Pollack et al. 1996; Alibert et al. 2005), which can lead to the formation of gas giants in a few million years, and the disk's gravitational instability (Boss 1997; Durisen et al. 2007), which can form massive planets on a very short timescale of a few thousand years (see Helled et al. 2014; Raymond et al. 2014 for reviews on those processes). Both agree on the formation of substellar companions from the circum-stellar accretion disk, but then differ depending on the initial environmental conditions in the disk, planet-disk, and planet-planet interactions.

Large planet-search surveys first focused on solar-type and very low-mass stars, leaving aside more massive stellar hosts that were more complex to observe and study. As the impact of the stellar mass on planet formation is still debated, it is of great interest to study the population of planets around intermediate-mass stars, that is in the 1.5 – 5  $M_{\odot}$  range. Such systems are especially useful to probe the two main competing formation models. In the early phase of the process, the stellar mass seems to have little effect on the protoplanetary disk formation and evolution; however, after 3 million years stars with masses > 2  $M_{\odot}$  start

**Table 1.** Planet-search programs monitoring evolved stars.

Survey	References
the Lick G- and K-giant survey	Frink et al. (2001); Hekker et al. (2006b)
the ESO planet search program	Setiawan et al. (2003)
the Okayama Planet Search Program	Sato et al. (2005)
with the collaborative survey "EAPS-Net"	Izumiura (2005)
the Tautenburg observatory Planet Search	Hatzes et al. (2005); Döllinger et al. (2007)
Retired A-stars and their companions	Johnson et al. (2006)
the CORALIE & HARPS search in open clusters	Lovis & Mayor (2007)
with the follow-up program	Delgado Mena et al. (2018)
the Penn States Torún Planet Search	Niedzielski et al. (2007)
with the follow-up program Tracking Advanced Planetary Systems	Niedzielski et al. (2015)
the BOAO K-giant survey	Han et al. (2010)
the Pan-Pacific Planet Search	Wittenmyer et al. (2011)
the Exoplanet aRound Evolved StarS project	Jones et al. (2011)
the Boyunsen Planet Search	Lee et al. (2011)

showing significant differences compared to lower mass stars, such as stronger radiation fields and higher accretion rates (Ribas et al. 2015). These impact the evolution of protoplanetary disks significantly, and by  $\sim 10$  Myr there are no more disks around those higher mass stars. The typical timescale of core accretion could become problematic for massive stars that have shorter disk lifetimes (Lagrange et al. 2000). However, searching for planets orbiting main-sequence stars of intermediate masses (A to mid-F types) proves to be a challenge for Doppler searches, mainly due to the too few absorption lines present in early-type dwarfs as a consequence of their high effective temperatures, and secondly due to the rotational broadening of the lines (typical rotational velocities of  $50\text{--}200\text{ km s}^{-1}$  for A-type stars,  $10\text{--}100\text{ km s}^{-1}$  for early-F stars (Galland et al. 2005)). A method to extract the radial-velocity from the spectrum in Fourier space was developed by Chelli (2000) and then adapted and applied to early-type stars by Galland et al. (2005). The typical radial-velocity uncertainties obtained were on the order of  $100\text{--}300$  and  $10\text{--}50\text{ m s}^{-1}$  (normalized to a signal-to-noise ratio (S/N) = 200) for A- and F-type stars, respectively. With this technique, the team confirmed the existence of the known planet around the F7V star HD 120136 (Tau Boo) announced by Butler et al. (1997). The orbital parameters from Galland et al. (2005) were consistent with the values previously found. These results confirmed the accuracy of the computed radial-velocities and the possibility to detect companions in the massive, giant planetary domain for A- and F-type stars with substantial  $v \sin i$ , using high-resolution, stable spectrographs such as HARPS.

On the other hand, stars will inflate during their evolution toward the red giant branch (RGB). The effective temperature thus reduces significantly, making many more absorption lines visible in the spectra. Moreover, the rotation of the star slows down, reducing the broadening effect on the lines and making them sharper. Those stars are thus suitable bright proxies for radial-velocity planet searches around intermediate-mass stars. The analysis and interpretation of the variability of radial-velocity time series of giant stars can, however, be challenging because of their intrinsic variability, which, moreover, can also be periodic (e.g., Hekker 2006, 2007). Disentangling stellar from potential planetary contributions represents a challenge in the search for long-period and low-mass companions around evolved stars.

Bringing observational constraints on the formation and evolution of planetary systems relies principally on the determination of orbital parameters such as semi-major axes and eccentricities. It also relies on the knowledge of host star properties such as

mass, radius, age, metallicity, and the abundances of individual elements. For giant stars, the mass and age are poorly constrained with the classical method of isochrone fitting because the evolutionary tracks in the HR diagram are too close to each other. The uncertainties on the observations (stellar magnitudes and colors) and systematics of the models lead to typical relative uncertainties on the stellar masses of  $80\text{--}100\%$ . Lovis & Mayor (2007), followed by Sato et al. (2007) and Pasquini et al. (2012), overcame this difficulty. They studied giant star populations in open clusters, for which better ages can be determined. This led them to better mass estimates from stellar evolution models (Lovis & Mayor (2007) using the Padova models at solar metallicity (Girardi et al. 2000)). More recently, GAIA DR2 unprecedented homogeneous photometric and astrometric data covering the whole sky allows for more precise age determination (e.g., Bossini et al. 2019 derived parameters such as age, distance modulus, and extinction for a sample of 269 open clusters).

In the late 1980s, a few surveys monitored giant star activity to better understand the origin of the observed large radial-velocity variations for late giant stars, with periods from days (Hatzes & Cochran 1994) to hundreds of days (Walker et al. 1989; Hatzes & Cochran 1993, 1999) and amplitudes of hundreds of  $\text{m s}^{-1}$  (Udry et al. 1999). Such a variability can be explained by a combination of stellar intrinsic activity such as oscillations, pulsations or the presence of substellar companions. Several surveys searching for stable reference stars reported that many giants show relatively small radial-velocity standard deviations for early giant stars:  $\sigma_{RV} \leq 20\text{ m s}^{-1}$  for several among the 86 K giants followed by Frink et al. (2001) and the 34 K giants observed by Hekker et al. (2006b). These results show that giant stars are suitable for the detection of substellar companions with radial-velocity measurements. It is worth mentioning the case of Gamma Cep here (Campbell et al. 1988), which is also considered as intrinsically variable despite the K1 giant spectral type.

Frink et al. (2002), as part of a radial-velocity survey of K giants (Frink et al. 2001), announced the detection of a  $8.9 M_{Jup}$  (minimal mass) companion orbiting the K2 III giant  $\iota$  Draconis with a period of 536 d period and an eccentricity of 0.70, making it the first substellar companion discovered orbiting a giant star. Since then, several radial-velocity surveys have been launched to follow evolved stars with intermediate masses. The list of these programs is presented in Table 1. As of November 2020, they

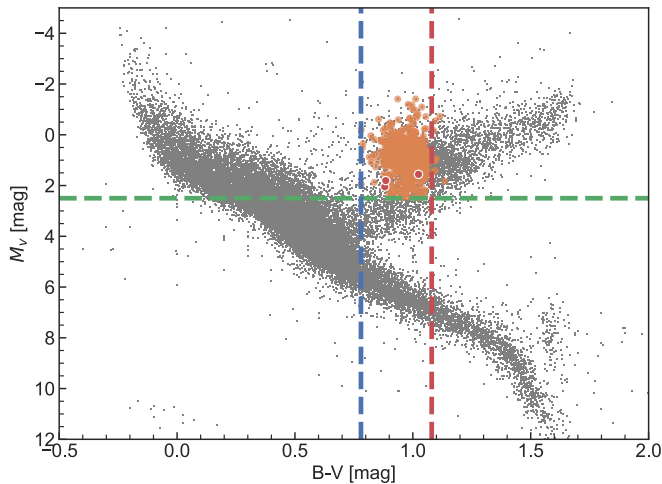


**Fig. 1.** Color-magnitude diagram from Hipparcos measurements (ESA 1997) for stars with parallax precisions better than 14% (in gray), with clear localization of our sample (in orange). The dashed lines represent the selection limits at absolute magnitude  $M_V < 2.5$  (green), and between the lower (red) and higher  $B - V$  values at 0.78 and 1.06. The planet host candidates presented in this paper (HD 22532, HD 64121, and HD 69123) are highlighted in red.

have led to the discovery of 186 substellar companions around evolved stars in 164 systems<sup>2</sup>.

In this context, a survey of a volume-limited sample of evolved stars of intermediate masses, the CORALIE radial-velocity Search for Companions Around Evolved Stars (CASCADES), was initiated in 2006. The sample is presented in Sect. 2, with the methods used to derive the stellar parameters described in Sect. 3. Section 4 describes the complete time series acquisition process and analysis, from the search for periodicities in the activity indicators to the Keplerian fitting of the radial velocities, which lead to orbital solutions of three newly discovered planetary companions in Sect. 5. Additional detections and statistical analysis of the survey will be presented in a series of subsequent publications. Finally, in Sect. 6 we discuss some implications of the first discoveries and provide concluding remarks in the broader context of the population of giant stars hosting substellar companions.

## 2. The CASCADES survey

### 2.1. Goals and sample definition

In the context described above, in 2006 we (i.e., Christophe Lovis and Michel Mayor) launched a precise radial-velocity survey of evolved stars of intermediate masses, which we refer to as "giant stars" in this paper. The main motivation was to better understand the formation of planetary systems and their evolution around stars more massive than the Sun by completing the existing statistical properties of giant host stars and their companions. To conduct a well-defined statistical study, we chose the following criteria for the definition of the sample:

We defined a volume-limited sample,  $d \leq 300$  pc. The selection was done in 2005 from the Hipparcos catalogue (ESA 1997). We only selected stars from the catalog with a precision on the

<sup>2</sup> The list was established from the NASA Exoplanet Archive, accessible at <https://exoplanetarchive.ipac.caltech.edu>, by selecting the hosts with  $\log g \leq 3.5$   $\text{cm s}^{-2}$ . The list thus contains giant and subgiant hosts.

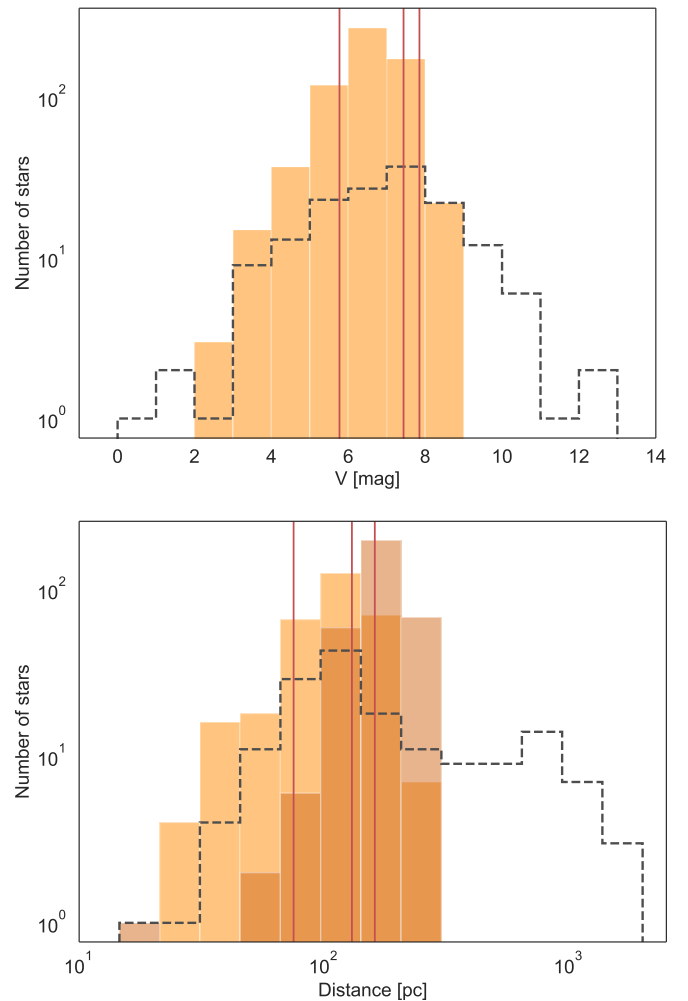


**Fig. 2.** Distributions of CASCADES survey sample (filled orange histogram), compared with the published giant stars known to host planet companions (dashed histogram). The top panel displays the apparent magnitude (TYCHO-2 catalog, Høg et al. (2000)) and the bottom one the distance (GAIA DR2, Bailer-Jones et al. (2018)). The CASCADES original 2006 sample and its 2011 extension are differentiated by lighter and darker orange shades, respectively. The positions of HD 22532, HD 64121, and HD 69123 are represented by red lines.

parallax better than 10%. To increase the statistics, the sample was extended in 2011 to targets with a parallax precision better than 14%. We selected stars with  $M_V < 2.5$  and  $B - V > 0.78$ , to avoid stars on the main sequence. We selected only early-type giants, with G and K spectral types and luminosity class III. To avoid later types, which are known to be intrinsically variable, we introduced a color cut-off at  $B - V < 1.06$ . We avoided close visual binaries for which we might have contamination by the secondary in the spectrograph fiber. The limit on the separation was set at  $6''$ . Finally, we selected stars observable by Euler, in the southern hemisphere, with a declination below  $-25^\circ$ , to be complementary to existing surveys in the north reaching down to  $\delta = -25^\circ$ .

The criteria and the final sample of 641 stars are represented in Fig. 1 displaying the Hipparcos color-magnitude diagram with the selected sample highlighted. In Fig. 2, we show the distribution of stellar apparent magnitudes and distances for the sample. We paid particular attention to the potential bias induced by the criterion on the parallax precision when carrying out the statistical study

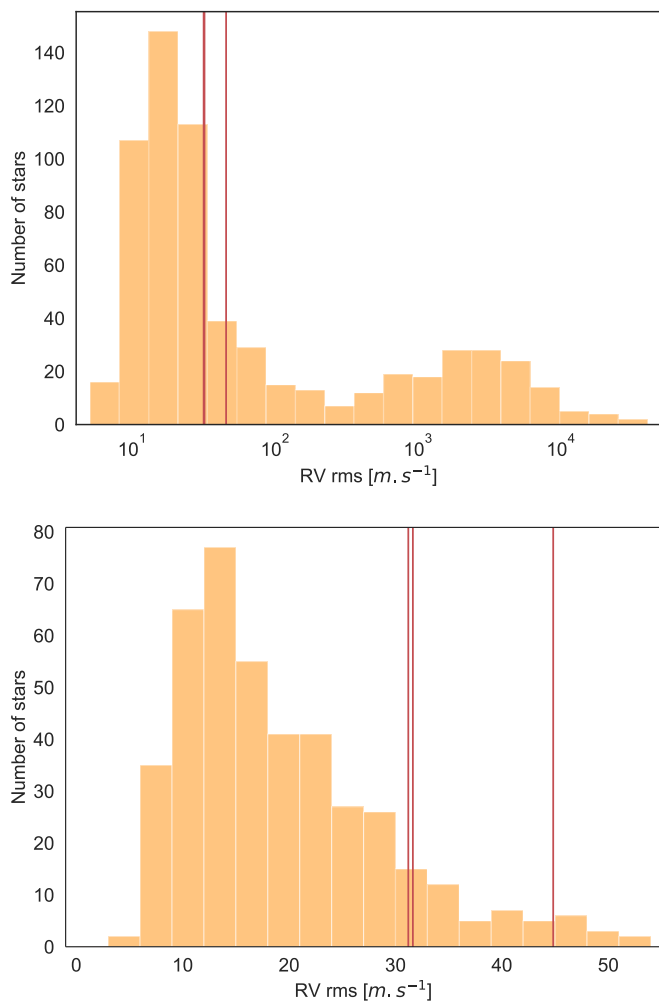


**Fig. 3.** Distribution of the radial-velocity dispersion observed for the stars in the sample. Top: Full range in logarithmic scale. Bottom: Zoomed-in image of smaller values, in linear scale. The positions of HD 22532, HD 64121, and HD 69123 are represented by red lines.

of the sample. Because of its size, timespan of observations, and the quantity and quality of the measurements, the above-defined planet search program is expected to significantly improve our knowledge of planetary systems around giant stars.

## 2.2. Instrument description and observations

Observations for this survey began at the end of 2006 and have been conducted since then with the CORALIE spectrograph on the 1.2-m Leonard Euler Swiss telescope located at La Silla Observatory (Chile). CORALIE is a 2-fiber-fed echelle spectrograph (2" fibers on the sky). It covers the 3880-6810 Å wavelength interval with 68 orders. The spectral resolution of the instrument was originally of 50 000. The observations are performed in the so-called simultaneous thorium mode<sup>3</sup>. In 2007 and 2014, CORALIE went through two significant hardware upgrades to improve the overall performance of the instrument, such as improving the throughput of the instrument (gain of 2 magnitudes) and increasing the resolution to 60 000. A Fabry-Perrot etalon

<sup>3</sup> A thorium-argon lamp illuminates fiber B at the same time as the star is observed on fiber A. Both spectra are recorded on the CCD.

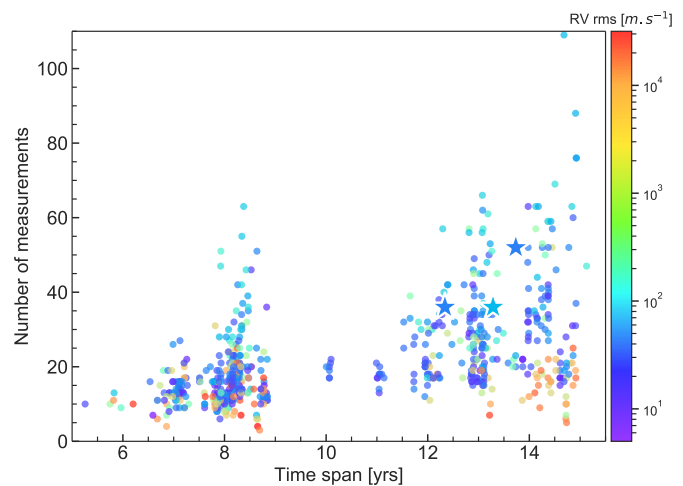


**Fig. 4.** Number of measurements per star in the sample plotted against the respective time span of the observations. The points are color-coded by the radial-velocity rms. The star markers represent HD 22532, HD 64121, and HD 69123.

was installed as well to replace the thorium-argon lamp used to track the variation of the spectrograph during the night. For simplicity, we refer to each dataset as CORALIE-98 (or COR98) for the first version of the instrument, CORALIE-07 (or COR07) for the 2007 upgrade and CORALIE-14 (or COR14) for the 2014 instrument upgrade. The instrumental precision evolved through these upgrades, from  $5 \text{ m s}^{-1}$  for COR98, to  $8 \text{ m s}^{-1}$  for COR07, and finally to  $2.5\text{-}3.2 \text{ m s}^{-1}$  for COR14. Complete information on instrumental aspects and the precisions reached are given in, for instance, [Queloz et al. \(2000\)](#); [Ségransan et al. \(2010, 2021\)](#).

Considering the size of the sample and the first results on the intrinsic variability of giant stars obtained by earlier surveys, we tried to optimize the exposure time in our program to match the limit set by stellar variation. Evolved stars often show distributions of the dispersion of radial-velocity time series ranging from  $\sim 5 \text{ m s}^{-1}$  up to a few hundreds of  $\text{m s}^{-1}$ , with a mode at  $\sim 15 \text{ m s}^{-1}$  ([Lovis & Udry 2004](#); [Hekker et al. 2006b](#); [Quirrenbach et al. 2011](#)). One of our objectives is also to test if this intrinsic limit can be lowered by modeling stellar variability, and thus to be able to recognise low-amplitude planet signatures. To reach a sufficient precision ( $\leq 2\text{-}3 \text{ m s}^{-1}$ ), exposure times between 3 and 5 minutes are adequate for these very bright stars.

The CASCADES survey is also interesting in the broader context of projects running on the telescope. The brightness of the stars in the sample makes them ideal back-up targets when weather conditions are unfavorable.

Almost 15 000 radial-velocity measurements have been obtained so far for the 641 stars of the sample. The study of the radial-velocity dispersion (see Fig. 3) confirms a distribution with a peak around  $13 \text{ m s}^{-1}$ , with values as low as  $\sim 4 \text{ m s}^{-1}$ . We also see a significant tail at higher values with a secondary peak around  $20 \text{ km s}^{-1}$  corresponding to binary systems.

Our observational effort is illustrated in Fig. 4, with the three host stars presented in this paper (located with a  $\star$  symbol) being among the most observed in the sample in terms of duration and number of data points. The program is continuing to obtain a minimum of 20 points per star and so can perform a solid statistical analysis of the sample.

### 3. Determination of stellar properties

#### 3.1. Spectroscopic parameters of the stars in the sample

The analysis of high-resolution spectra can provide reliable stellar parameters such as effective temperature  $T_{eff}$ , surface gravity  $\log g$ , and iron metallicity ratio  $[Fe/H]$  (which we refer to as metallicity in this paper for simplicity). Alves et al. (2015) presented a catalog of precise stellar atmospheric parameters and iron abundances for a sample of 257 G and K field evolved stars, all of them part of our sample, using UVES and CORALIE spectra. The approach, based on Santos et al. (2004), uses the classic curve-of-growth method. The equivalent width of a set of Fe I and II lines is measured and their abundances are calculated. Then, the stellar parameters are derived when excitation and ionization balances are satisfied simultaneously under the assumption of local thermodynamic equilibrium. For a detailed description of the method and the results, we direct the reader to Santos et al. (2004); Sousa (2014); Alves et al. (2015).

Before 2014, the CORALIE spectra obtained for precise RV measurements were polluted by the strongest lines of the Thorium-Argon spectrum from the calibration fiber, and thus they were not suitable for a precise spectroscopic analysis. Dedicated additional spectroscopic observations (without calibration) were then obtained for our sample stars. After the CORALIE upgrade in 2014, the calibration spectrum from the Fabry-Perrot etalon was no longer polluting the stellar spectrum, and the observations of radial-velocity measurements can also be used for the spectroscopic analysis. We stacked the CORALIE-14 spectra from all stars in our sample to reach a high enough S/N (the median S/N of the master spectra is about 170), and we derived the spectroscopic parameters  $T_{eff}$ ,  $\log g$  and  $[Fe/H]$  using the ARES(Sousa et al. 2007, 2015) + MOOG (Snedden 1973) methodology following Sousa (2014). For most of the stars, with  $T_{eff} < 5200$  K, the iron line list presented in Tsantaki et al. (2013) was used. While for the hotter stars we used the standard line list presented in Sousa et al. (2008). We then compared these results with the ones presented in Alves et al. (2015) for the subsample of 254 common stars. Figure 5 shows the good agreement found between the parameters obtained from the UVES and CORALIE spectra: in the case of metallicity, we observe an apparent positive offset of the order of the dispersion of the data around the 1:1 correlation,  $\sim 0.04$  [dex] in favor of our estimation. More than 50% of the subsample stars are inside the  $1\sigma$  region and 90% are inside  $2\sigma$ . These results confirm the quality of the CORALIE-14 spectra to extract reliable atmospheric parameters from them.

#### 3.2. Stellar luminosities, radii, and masses

We derived the luminosity  $L$  for the stars in our sample using the Gaia DR2 parallaxes corrected by Bailer-Jones et al. (2018)<sup>4</sup>, V-band magnitudes from Høg et al. (2000), and the bolometric correction  $BC$  of Alonso et al. (1999)<sup>5</sup>. We then used this luminosity and the spectroscopic effective temperature  $T_{eff}$  to compute the stellar radii using the Stephan-Boltzmann relation. The uncertainties of the radii were estimated using a Monte Carlo approach. We compared our temperatures and radii with

the GAIA DR2 values and found them to be in good agreement, as illustrated in Fig. 6.

The derived luminosities and spectroscopic effective temperatures are plotted in the Hertzsprung-Russell diagram in Fig. 7, together with the stellar evolutionary tracks at solar metallicity of Pietrinferni et al. (2004)<sup>6</sup>. Those were used to estimate the masses of our stars using the SPInS software (Lebreton & Reese 2020)<sup>7</sup>. The approach compares the luminosity, effective temperature, logarithm of surface gravity, and  $[Fe/H]$  of individual objects to theoretical evolutionary tracks and accounts for the observational errors in these four quantities. Giant stars are located in the area of the Hertzsprung-Russell diagram where individual evolutionary tracks are close to each other; thus, the derived precisions on the stellar masses might be overestimated. However, in our sample, the degeneracy between the horizontal branch (HB) and RGB is not too pronounced. Comparisons with masses derived from detailed asteroseismic modeling (see Sect. 3.3) show some small differences. These discrepancies mainly originate from the use of a fixed enrichment law in the grid of Pietrinferni et al. (2004), such that the chemical composition of the stars of our sample is fully determined from the determination of  $[Fe/H]$  in our modeling using SPInS. This was not the case for the seismic modeling pipeline, where the additional constraints justified allowing for an additional free parameter. Thus, solutions with a chemical composition deviating from a fixed enrichment law where helium and metal abundances are tied together were possible outcomes of the modeling procedure. This is particularly visible for the two stars with  $Fe/H \sim -0.2$  studied in Sect. 3.3 (HD 22532 and HD 64121), for which the asteroseismic analysis reveals an initial helium abundance slightly higher than the solar one despite their subsolar metallicity. This situation of course cannot be reproduced by models with an initial helium abundance fixed by the metallicity, which then leads to an overestimation of the stellar mass determined by SPInS to compensate for the incorrect helium abundance and reproduce the observed location in the HR diagram.

Nevertheless, we can consider that these fits still allow us to globally estimate the stellar masses of our sample of stars. The obtained distribution for all stars is shown in Fig. 8. The median of the distribution is found around  $2.1 M_{\odot}$ , corresponding to intermediate-mass stars. However, as mentioned above, some uncertainty on the evolutionary stage of a subsample of stars of our sample could have affected our determinations, especially if we consider deviations from a given chemical enrichment law. Indeed, some stars of our sample identified here as being around  $\approx 2.0 M_{\odot}$  on the RGB could actually be low-mass stars in the red clump. This degeneracy could be lifted using asteroseismic observations of dipolar oscillation modes that allow us to unambiguously determine the evolutionary stage of these stars (Beck et al. 2011; Bedding et al. 2011).

Table 2 shows example lines of the complete set of stellar parameters for our sample, available online<sup>8</sup>. We also illustrate our results in Fig. 8. The metallicity distribution decreases with increasing  $[Fe/H]$  for  $[Fe/H] > 0.0-0.1$ , similarly to the metallicity distribution (Santos et al. 2001) of a large, volume-limited sample of dwarf stars in the solar neighborhood, included in the CORALIE survey (Udry et al. 2000). We observe that our sample of giants is lacking the metal-rich and very metal-poor stars. This

<sup>4</sup> Bailer-Jones et al. (2018) provided purely geometric distance estimates by using an inference procedure that accounts for the nonlinearity of the transformation (inversion of the parallax) and the asymmetry of the resulting probability distribution.

<sup>5</sup> Considering the short distance of the stars of the sample, the extinction was not taken into account.

<sup>6</sup> Available on the BaSTI database <http://basti.ao-teramo.inaf.it>.

<sup>7</sup> <https://dreese.pages.obsppm.fr/spins/index.html>, which employs a global Markov Chain Monte Carlo (MCMC) approach taking into account the different timescales at various evolutionary stages and interpolation between the tracks.

<sup>8</sup> Available at CDS and <https://dace.unige.ch>.

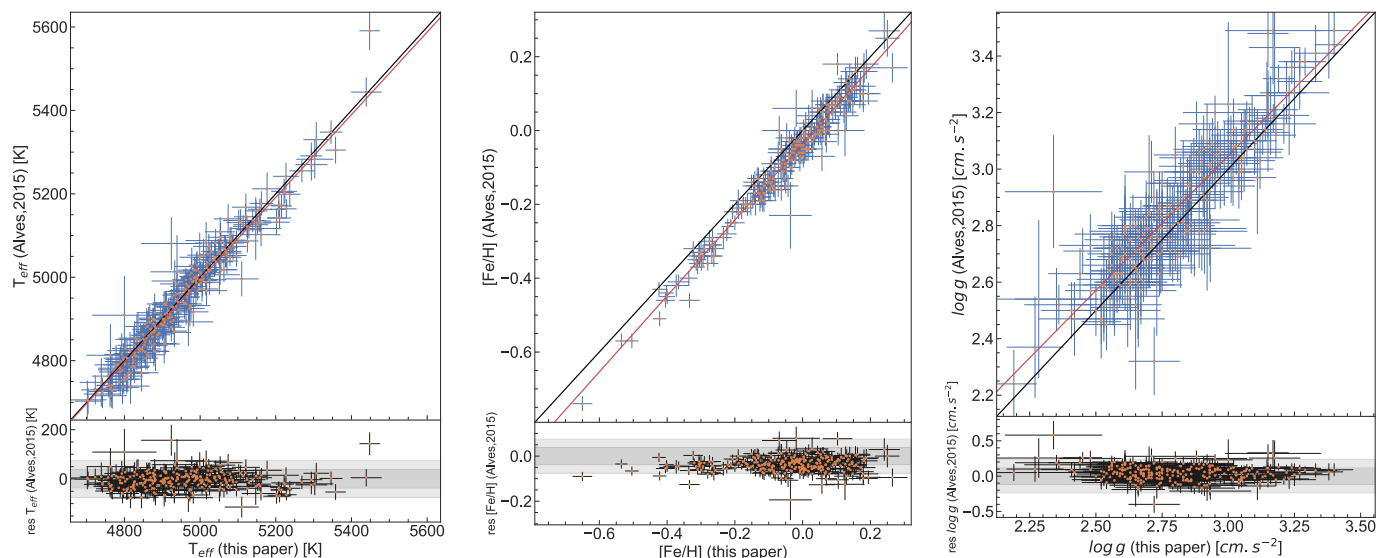


**Fig. 5.** Comparison plots of spectroscopic parameters extracted from CORALIE (this paper) and UVES (Alves et al. 2015) spectra of the subsample of 254 stars in common. The black diagonal line represents the 1:1 correlation, and the red line represents the linear fit of the data. At the bottom of each figure, the residuals compared to the 1:1 correlation are shown, with their 1 and  $2\sigma$  dispersions represented by the shaded regions. Left: Effective temperatures seem to be perfectly correlated, with a dispersion of  $\sim 38$  K. Middle: Metallicity ratio of iron [Fe/H] shows an apparent positive offset of the order of the dispersion of the data around the 1:1 correlation,  $\sim 0.04$  [dex] in favor of our estimation. More than 50% of the subsample is inside the  $1\sigma$  region and 90% inside the  $2\sigma$ . Right: Logarithm of the surface gravity shows a good correlation, with an offset  $\sim 0.05$   $cm.s^{-2}$  lower than apparent dispersion of the data around the 1:1 correlation. More than 70% of the subsample is inside the  $1\sigma$  region.

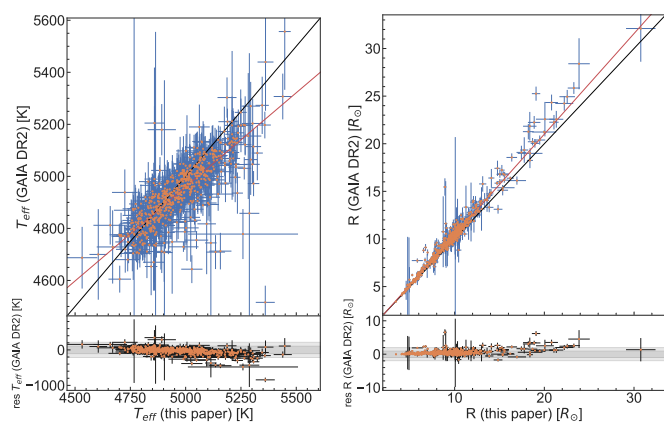


**Fig. 6.** Comparison plots of photometric (from Brown et al. 2018) and spectroscopic (from this paper) determinations of the effective temperatures and the stellar radii. The black diagonal line represents the 1:1 correlation and the red line represents the linear fit of the data. At the bottom of each figure, the residuals compared to the 1:1 correlation are shown, with their 1 and  $2\sigma$  dispersions represented by the shaded regions. Left: Effective temperatures seem to show a linear trend, but this is not significant compared to the dispersion of the data of  $\sim 110$  K, inside which more than 85% of the data is located. Right: Radii are in good agreement but show an apparent trend and increasing dispersion for masses above than  $\sim 15 M_{\odot}$ .

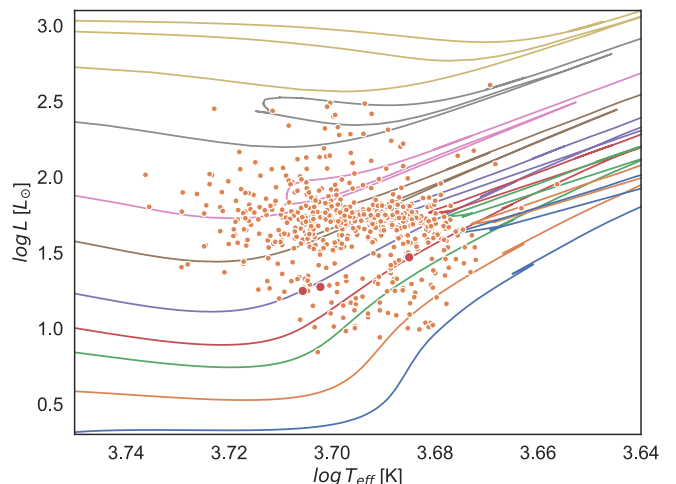


**Fig. 7.** Positions in Hertzsprung-Russell diagram of the subsample of 620 stars for which we derived spectroscopic parameters. The three host stars we focus on in the present paper are highlighted as red dots. We adopted the luminosities obtained with the method described in Sect. 3.2. The evolutionary tracks are from models of Pietrinferni et al. (2004) for different stellar masses (1.0, 1.2, 1.5, 1.7, 2.0, 2.5, 3.0, 4.0, and  $5.0 M_{\odot}$  from bottom to top). They are for models with solar metallicity.

tendency has been observed in many studies (e.g., Luck & Heiter 2007; Takeda et al. 2008; Ghezzi et al. 2010; Adibekyan et al. 2015; Adibekyan 2019). It may be related to the fact that giants, most of them being more massive, are younger than their dwarf counterparts. They thus do not have time to migrate far from the inner to the outer disks of the galaxy during their short lifetimes (Wang & Zhao 2013; Minchev et al. 2013). Adibekyan (2019) also addresses the role of the age-metallicity dispersion relation

(da Silva et al. 2006; Maldonado et al. 2013), as well as potential selection effects due to B-V color cut-off (Mortier et al. 2013), which excludes low-log-g stars with high metallicity and high-log-g stars with low metallicity. We illustrate this effect in Fig. 8, in the same way as (Adibekyan et al. 2015), by drawing diagonal lines that show the biases in the sample due to the color cut-off. We also represent the area that would correspond to an unbiased subsample inside a cut rectangle (red dashed rectangle). We will

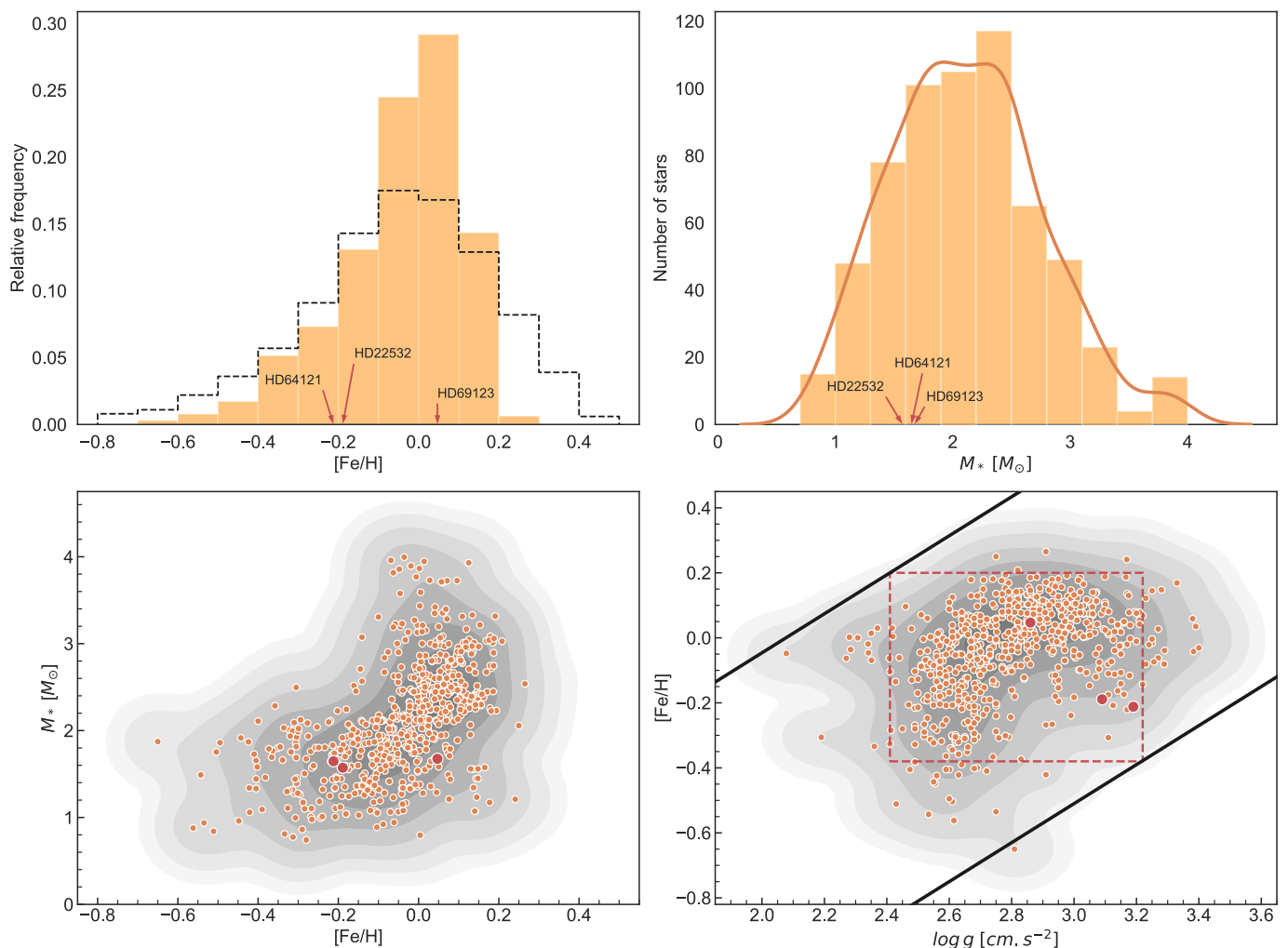


**Fig. 8.** Distributions and relations between stellar parameters for our subsample of 620 stars. Top left: Metallicity distribution of the stars of our sample (colored in orange) compared with the same distribution for the  $\sim 1000$  stars (dashed histogram) in the CORALIE volume-limited sample (Udry et al. 2000; Santos et al. 2001). Top right: Distribution of the stellar masses obtained from track fitting. The corresponding kernel density estimation is overplotted in orange, using a Gaussian kernel. Bottom left: Mass vs. metallicity relation. (bottom right) Metallicity vs. logarithm of surface gravity. The two black lines were drawn by eye and show the biases in the samples due to the B-V cut-off. The red-dashed rectangle delimits the area of the potential unbiased subsample. The three planet hosts presented in this paper are represented by red dots.

perform a detailed statistical study of the stellar parameters of our sample in future work.

### 3.3. Asteroseismic masses for the three planet hosts

To go further and improve the mass estimation for the host star, we performed a detailed seismic analysis of the TESS short-cadence photometric data (Ricker et al. 2014), following the methodology of Buldgen et al. (2019). This asteroseismology approach has the considerable advantage of leading to a highly precise and accurate mass estimate independently of any stellar evolution models. We used the method to extract masses for the three stellar hosts presented in this paper (see Table 3) to obtain a better estimation of the minimum mass of their planetary companions. The seismic masses can also be used as a benchmark to assess the accuracy of the masses obtained from evolutionary models, which in this case appear to be overestimated by an offset of  $\sim 0.3\text{--}0.4 M_{\odot}$  but are consistent within  $3\text{--}4 \sigma$ . This aspect will be addressed in a forthcoming paper once more asteroseismic masses are available. In practice, the mass estimates we present here are a result of the

combination of seismic inversions of the mean density with the values of the stellar radii derived from GAIA parameters. The seismic inversion of the mean density was carried out following the methodology of Buldgen et al. (2019) and validated on eclipsing binaries. This estimate still depends on the seismic data, as well as the details of the determination of the radii from GAIA and spectroscopic data, such as the bolometric corrections and extinction laws. An in-depth description of the data extraction and seismic modeling, as well as an analysis of the orbital evolution and atmospheric evaporation of the planetary systems, can be found in a companion paper (Buldgen et al. 2021). In Table 3, we summarize the spectroscopic parameters of the three stellar hosts announced in this paper and their masses derived from evolutionary tracks and asteroseismology.

## 4. Data acquisition and analysis

### 4.1. Data acquisition and processing

For each target, we collected several tens of radial-velocity data over a median time span of 13 years, with a typical S/N = 70

**Table 2.** Example entries of the table of stellar parameters for the complete sample, available online at CDS.<sup>8</sup>

HD	Sp. Type	$V$ [mag]	$B - V$ [mag]	$BC$ [mag]	$\pi$ [mas]	$d$ [pc]	$M_V$ [mag]	$Bp - Rp$ [mag]	$G$ [mag]	$T_{eff}$ [K]	$log g$ [cm s <sup>-2</sup> ]	$[Fe/H]$ [dex]	$M_*$ [M <sub>⊙</sub> ]	$L_*$ [L <sub>⊙</sub> ]	$R_*$ [R <sub>⊙</sub> ]
	[1]	[2]	[2]	[3]	[4]	[5]	[2,4,5]	[4]	[4]	[6]	[6]	[6]	[7]	[2,3,4]	[2,3,4,6]
496	K0III	3.88 ± 0.01	1.00 ± 0.01	-0.312 ± 0.016	24.20 ± 0.29	41.3 <sup>+0.5</sup> <sub>-0.5</sub>	0.80 ± 0.03	1.218 ± 0.006	0.42 ± 0.03	4858 ± 41	2.56 ± 0.10	-0.01 ± 0.03	1.93 ± 0.23	50.44 ± 1.46	10.03 ± 0.22
636	K1/K2III	5.29 ± 0.01	1.03 ± 0.01	-0.303 ± 0.019	12.60 ± 0.08	79.2 <sup>+0.5</sup> <sub>-0.5</sub>	0.80 ± 0.02	1.177 ± 0.005	0.47 ± 0.02	4879 ± 51	2.78 ± 0.15	0.19 ± 0.04	2.23 ± 0.09	50.47 ± 1.17	9.94 ± 0.24
770	K0III	6.54 ± 0.01	1.04 ± 0.02	-0.317 ± 0.017	7.22 ± 0.04	137.9 <sup>+0.7</sup> <sub>-0.7</sub>	0.84 ± 0.02	1.178 ± 0.003	0.54 ± 0.01	4845 ± 45	2.66 ± 0.10	-0.08 ± 0.04	1.91 ± 0.17	49.14 ± 1.04	9.95 ± 0.21
...	...	...	...	...	...	...	...	...	...	...	...	...	...	...	...
224949	K0III	7.10 ± 0.01	0.99 ± 0.02	-0.338 ± 0.013	5.73 ± 0.05	173.7 <sup>+1.4</sup> <sub>-1.4</sub>	0.90 ± 0.02	1.183 ± 0.004	0.60 ± 0.02	4795 ± 32	2.49 ± 0.09	-0.33 ± 0.03	1.30 ± 0.06	47.32 ± 1.07	9.97 ± 0.17

[1] - HIPPARCOS catalog (ESA 1997), [2] - TYCHO-2 catalog (Høg et al. 2000), [3] - Alonso et al. (1999), [4] - GAIA DR2 (Brown et al. 2018), [5] - Bailer-Jones et al. (2018), [6] - this paper (see Sect. 3.1), [7] - this paper, with evolutionary tracks from Pietrinferni et al. (2004).

**Table 3.** Observed and inferred stellar parameters.

	ref.	HD 22532	HD 64121	HD 69123
TIC		200851704	264770836	146264536
GAIA DR2		4832768399133598080	5488303966125344512	5544699390684005248
Sp. Type	[1]	G8III/IV	G8/K0III	K1III
$V$	[mag]	7.85 ± 0.01	7.44 ± 0.01	5.77 ± 0.01
$B - V$	[mag]	0.89 ± 0.02	0.86 ± 0.02	1.02 ± 0.01
$BC$		-0.250 ± 0.013	-0.238 ± 0.012	-0.318 ± 0.016
$\pi$	[mas]	6.18 ± 0.03	7.67 ± 0.03	13.28 ± 0.06
$d$	[pc]	161.2 <sup>+0.7</sup> <sub>-0.7</sub>	130.0 <sup>+0.5</sup> <sub>-0.5</sub>	75.1 <sup>+0.4</sup> <sub>-0.4</sub>
$M_V$	[mag]	[2,4,5]	1.81 ± 0.01	1.87 ± 0.01
$Bp - Rp$	[mag]	[4]	1.087 ± 0.002	1.076 ± 0.004
$M_G$	[mag]	[4]	1.56 ± 0.01	1.60 ± 0.01
$T_{eff}$	[K]	[4]	5067 <sup>+59</sup> <sub>-22</sub>	5066 <sup>+58</sup> <sub>-60</sub>
		[6]	5038 ± 24	5078 ± 22
$log g$	[cm s <sup>-2</sup> ]	[6]	3.09 ± 0.07	3.19 ± 0.06
$[Fe/H]$	[dex]	[6]	-0.19 ± 0.02	-0.21 ± 0.02
$M_*$	[M <sub>⊙</sub> ]	[7]	1.57 ± 0.07	1.64 ± 0.06
		[8]	1.20 ± 0.05	1.18 ± 0.05
$L_*$	[L <sub>⊙</sub> ]	[2,3,4]	18.80 ± 0.33	17.70 ± 0.30
$R_*$	[R <sub>⊙</sub> ]	[2,3,4,6]	5.69 ± 0.07	5.44 ± 0.07
				7.72 ± 0.15

[1] - HIPPARCOS catalog (ESA 1997), [2] - TYCHO-2 catalog (Høg et al. 2000), [3] - Alonso et al. (1999), [4] - GAIA DR2 (Brown et al. 2018), [5] - Bailer-Jones et al. (2018), [6] - this paper (see Sect. 3.1), [7] - this paper, with evolutionary tracks from Pietrinferni et al. (2004), [8] - Buldgen et al. (2021).

for an exposure time between 180 and 300 s<sup>9</sup>. Tables A.1–A.3 give the list of these measurements with their instrumental error bars. We first analyzed the radial-velocity time series using the radial-velocity module of the Data & Analysis Center for Exoplanets (DACE) web platform,<sup>10</sup> which provides an open access to a wide range of exoplanets' observational and theoretical data with the corresponding data visualization and analysis tools. The formalism of the radial-velocity data analysis implemented in DACE is described in Ségransan et al. (submitted, Appendix A) and is mainly based on algorithms presented in Díaz et al. (2014) and Delisle et al. (2016, 2018).

Our general approach for a periodic signal search is the following. For each time series, we follow an iterative process consisting of looking for successive significant dominant peaks in the periodograms of the corresponding radial-velocity residuals. At each step, the radial-velocity residuals are computed by readjusting the model composed of the N-independent Keplerians, potential linear or quadratic drift terms to fit long-term trends, the individual instrumental offsets, and additional noise. We fit a combination of

white noise terms corresponding to individual instrumental precisions<sup>11</sup> and a global noise term attributed to intrinsic stellar jitter. This approach allows us to obtain an idea of how much noise can be attributed to stellar physics; however, one must be aware of the degeneracy between those two sources of noise, which is only partially lifted by using strong priors on the instrumental noise. The final error bars on the velocities correspond to the quadratic sum of the error computed by the data reduction software, the instrumental noise and the stellar jitter. We proceeded with the periodicity search by computing the periodogram of the data in the 1 – 10 000 days<sup>12</sup> range and using the false alarm probability (FAP) to assess the significance of the signal, following the formalism of Baluev (2008). Significant signals can have different origins, and they are discussed in Sect. 4.2.

<sup>9</sup> Following the 2007 and 2014 upgrades, we have to fit a small radial-velocity offset between the three versions of the CORALIE instrument, the values of the offset depending on several aspects such as the considered star or the correlation mask used. We thus consider the three versions of CORALIE as three different instruments.

<sup>10</sup> <https://dace.unige.ch/radialVelocities/>.

<sup>11</sup> The instrumental precisions are well constrained for each version of CORALIE, calibrated on non-active stars:  $\sigma_{COR98} = 5.0 \pm 0.5 \text{ m s}^{-1}$ ,  $\sigma_{COR07} = 8.0 \pm 0.5 \text{ m s}^{-1}$ , and  $\sigma_{COR14} = 3.0 \pm 0.5 \text{ m s}^{-1}$ . Those values are used as priors on the instrumental noise terms in Sect. 5.

<sup>12</sup> Using the algorithm implemented on DACE (see Delisle et al. (2020)) and setting the upper bound of the periodogram at approximately twice the time span of the survey.



#### 4.2. Stellar activity and line profile analysis

Stellar activity in giant stars originates from different phenomena. Short period modulations of the order of hours to days (first discussed by Walker et al. (1989); Hatzes & Cochran (1993, 1994)) are understood to be the result of solar-like radial pulsations (p, g, or mixed modes) (Frandsen et al. 2002; De Ridder et al. 2006; Hekker 2006). Concerning longer period variations, mechanisms such as magnetic cycles (Santos et al. 2010; Dumusque et al. 2011), rotational modulation of features on the stellar surface (star spots, granulation, etc. (Lambert 1987; Larson et al. 1993; Delgado Mena et al. 2018)), beating of modes, or a combination of all three are to be considered. Non-radial oscillations have also been discussed (Hekker et al. 2006a) and confirmed by De Ridder et al. (2009); Hekker & Aerts (2010) as a source of periodic modulation of the spectroscopic cross-correlation profile. Those modes can have lifetimes of up to several hundreds of days (Dupret et al. 2009).

The careful monitoring of the spectral line profile via the cross-correlation function (CCF) and of the chromospheric activity indicators is essential to help distinguish between planetary signals and stellar-induced variations of the radial velocities.

Our estimate of the star's radial velocity is based on the CCF technique (Griffin 1967; Baranne et al. 1979; Queloz et al. 2001), which creates a sort of mean spectral line from the thousands of lines used in the correlation, and of significantly higher S/N compared to a single line. In order for stellar activity to significantly impact the CCF profile, and thus the radial-velocity value, it would have to affect the majority of the spectral lines. Such an effect could cause deformations in the line profile and possibly mimic a planetary signal. Computing the contrast, radial-velocity, full width at half maximum (FWHM), and the bisector inverse span (BIS), which are linked to the first four moments of the line profile, gives enough information to precisely control the evolution of the profile along the time series (Aerts & Eyser 2000).

Magnetic activity enhances the emission from the stellar corona and chromosphere, resulting in emissions in the X-Ray and UV regions, as well as emissions in the cores of the *H&K Ca II* lines and *H $\alpha$* . The *H $\alpha$*  activity index is sensitive to solar prominences and chromospheric activity. The reversal emission in the line core of *Ca II H&K* (S-index) (Wilson 1978), which measures the contributions from the stellar photosphere and chromosphere, and the  $\log R'_{HK}$  activity index, which measures the chromospheric contribution of the *H&K Ca* lines excluding the photospheric component, cannot be directly computed from the CORALIE spectra in a reliable way, because of the low S/N in this part of the spectra.

The time series and corresponding periodograms of those line profiles and of the *H $\alpha$*  chromospheric indicator (following the method described in Boisse et al. 2009; Gomes da Silva et al. 2011) are produced systematically to check for any signs of periodicity and a possible origin of the radial-velocity variations. Correlations between these indicators and radial velocities were also checked. Causes such as stellar pulsations can be ruled out by comparing the behavior of line profiles from different spectral regions; for pulsating stars, the temporal and phasing behavior of the moments should remain the same for any spectral region (a signature should also be present in the BIS (Hatzes & Cochran 1999)). For detailed examples, we invite the reader to consult the analyses of Briquet et al. (2001) or Briquet et al. (2004), which attempted to discriminate between stellar pulsation and rotational modulation (presence of stellar spots) as the source of observed periodic variability, using *Si II* and *He I* lines in slow pulsating B stars. In the case of rotational modulation, the BIS and the S-

index should vary in phase and with the same period as the radial-velocities, which is a period that should also correspond to the stellar rotation period. However, phase shifts have been observed, for example, in the case of the G2 dwarf HD 41248 (Santos et al. 2014). The star exhibits a 25 day periodicity in the radial-velocity, FWHM, and  $\log R'_{HK}$  time series, probably explained by rotational modulation combined with a strong differential rotation of the star. We should, however, stress here that giant stars are still not fully understood, and we have to keep in mind that the absence of periodic signals in line-shape variations does not mean for sure that the radial-velocity signal is induced by a planetary companion. It remains, however, our best interpretation of the observations.

### 5. Analysis of individual systems: Orbital solutions

Following the approach described in Sect. 4.1, we analyzed the long time series of observations obtained for the three targets presented in this paper. The final parameters of each system were computed using the MCMC algorithm implemented in DACE (developed by Díaz et al. (2014, 2016)) to probe the complete parameter space, with 1.6 million iterations. We fit the following parameters for the Keplerian model:  $\log P$  and  $\log K$  to better explore ranges of several orders of magnitude with a uniform prior.  $\sqrt{e \cos \omega}$  and  $\sqrt{e \sin \omega}$  to obtain a uniform prior for the eccentricity. Finally, we obtained  $\lambda_0$ , the mean longitude at epoch of reference (i.e.,  $BJD = 2\,455\,500$  [d]), with a uniform prior. We used a uniform prior for the COR07 offset of reference, and Gaussian priors for the relative offsets between COR07 and COR98/14:  $\Delta RV_{COR98-COR07}: \mathcal{N}(0, 4) \text{ m s}^{-1}$  and  $\Delta RV_{COR14-COR07}: \mathcal{N}(14, 4) \text{ m s}^{-1}$ . We also used Gaussian priors for the instrumental noise:  $\sigma_{COR98}: \mathcal{N}(5, 1) \text{ m s}^{-1}$ ,  $\sigma_{COR07}: \mathcal{N}(8, 1.5) \text{ m s}^{-1}$ , and  $\sigma_{COR14}: \mathcal{N}(3, 0.5) \text{ m s}^{-1}$ . Finally, we used a uniform prior for the stellar jitter parameter.

For all three targets, the fit instrumental noises (on top of the photon noise) are in the range of the individual instrumental precisions. In the case of HD 64121, the fit stellar jitter clearly dominates over the instrumental precision, with a level of  $\sim 17 \text{ m s}^{-1}$ . For each time series, we checked for periodicities and correlations in the activity-related products of the high-resolution spectra mentioned above.

#### 5.1. HD 22532

For HD 22532<sup>13</sup>, we detect a  $\sim 873$  day periodic variation of the radial velocities, which, fit by a Keplerian model, corresponds to a planet in a quasi-circular orbit, 1.9 au away from its star, and with a semi-amplitude of  $40 \text{ m s}^{-1}$  corresponding to a minimum mass of  $2.1 M_J$  (using  $M_\star = 1.2 M_\odot$  from Table 3). We observe in the periodogram of the *H $\alpha$*  activity index of HD 22532 (see bottom periodogram in Fig. 9) a non-significant peak at  $\sim 810$  days, with a FAP level well below 10%, which is at the same level as the higher frequency white noise. We checked for a linear correlation with the radial-velocities, and the weighted Pearson coefficient was found as low as  $R_P = -0.396 \pm 0.068$ . We also computed the weighted Spearman's rank  $R_S = 0.411 \pm 0.066$ , which is also considered a low correlation. The important dispersion of the *H $\alpha$*  data points and the low significance of a period approximately 60 days shorter than the one detected in the radial velocities indicates that those variations are most likely not at the origin of - nor are they linked to - the radial-velocity signal.

<sup>13</sup> TIC 200851704 ; GAIA DR2 4832768399133598080

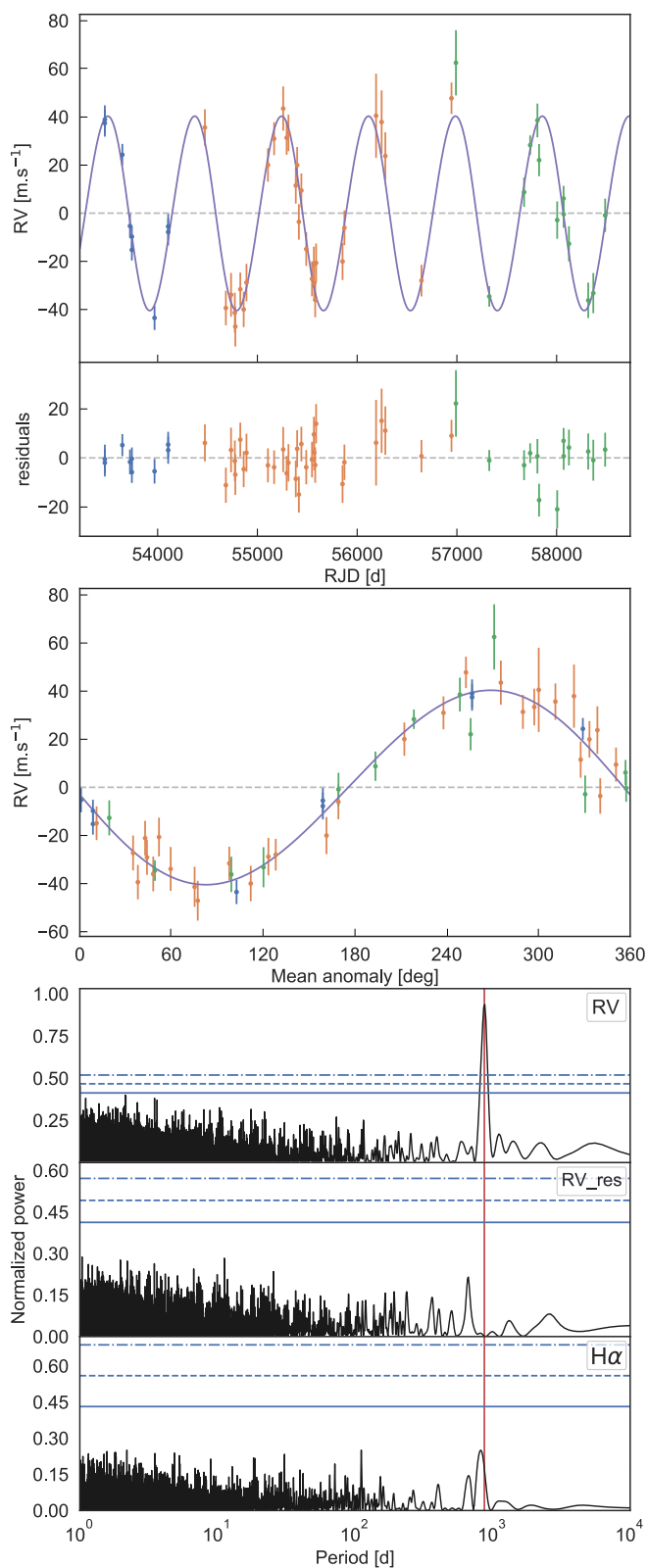


**Fig. 9.** Top panel: Radial velocities of HD 22532 from CORALIE (COR98 in blue, COR07 in orange and COR14 in green) with the best Keplerian model superimposed (solid line), and corresponding residuals around the solution. Second panel: Phased radial-velocity solution. Third panel: Periodograms of the radial-velocity time series, the residuals of the radial-velocities after subtraction of the fit periodic signal, and the periodogram of the  $H\alpha$  activity index time series. The red vertical line indicates the period of the orbital solution (872.6 days). Horizontal lines are the FAP levels at 10% (continuous), 1% (dashed), and 0.1% (dotted-dashed).

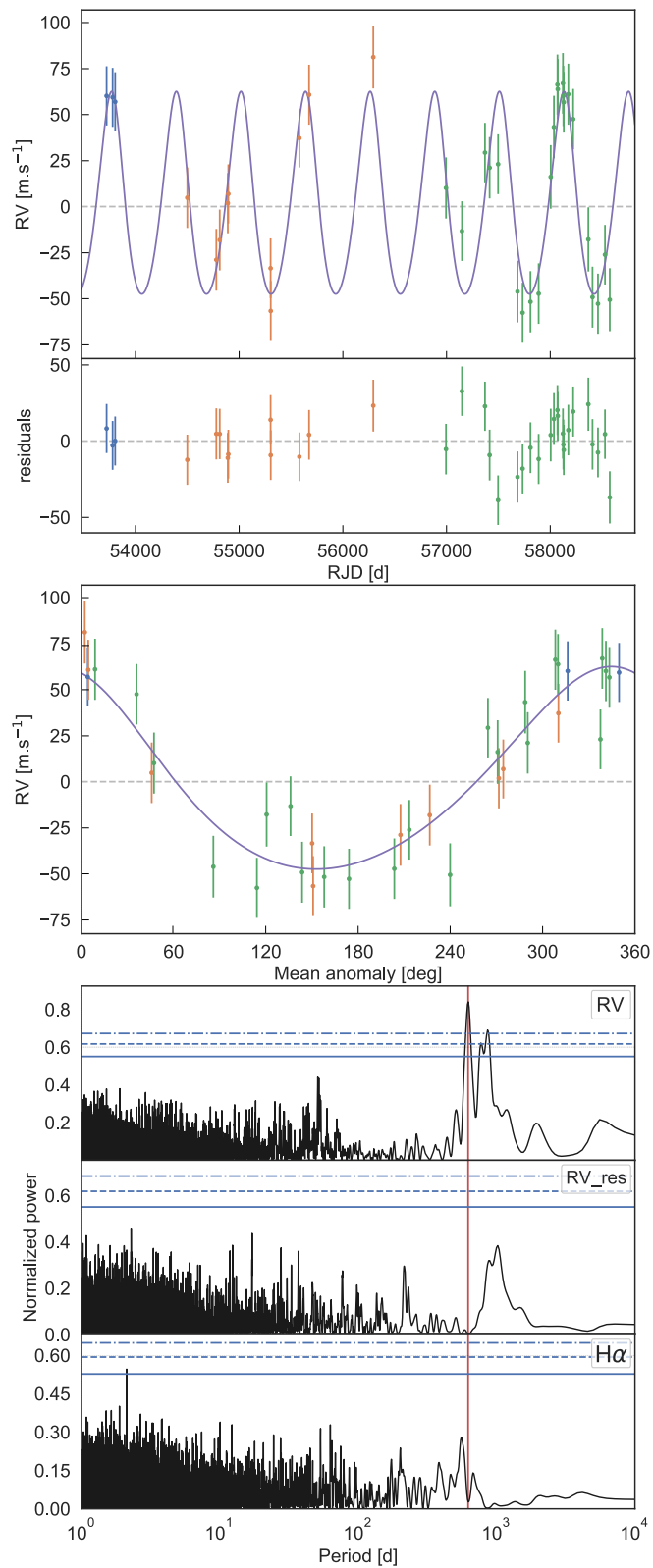


**Fig. 10.** Same as Fig. 9, but for HD 64121. The period of the best solution is 623.0 days.

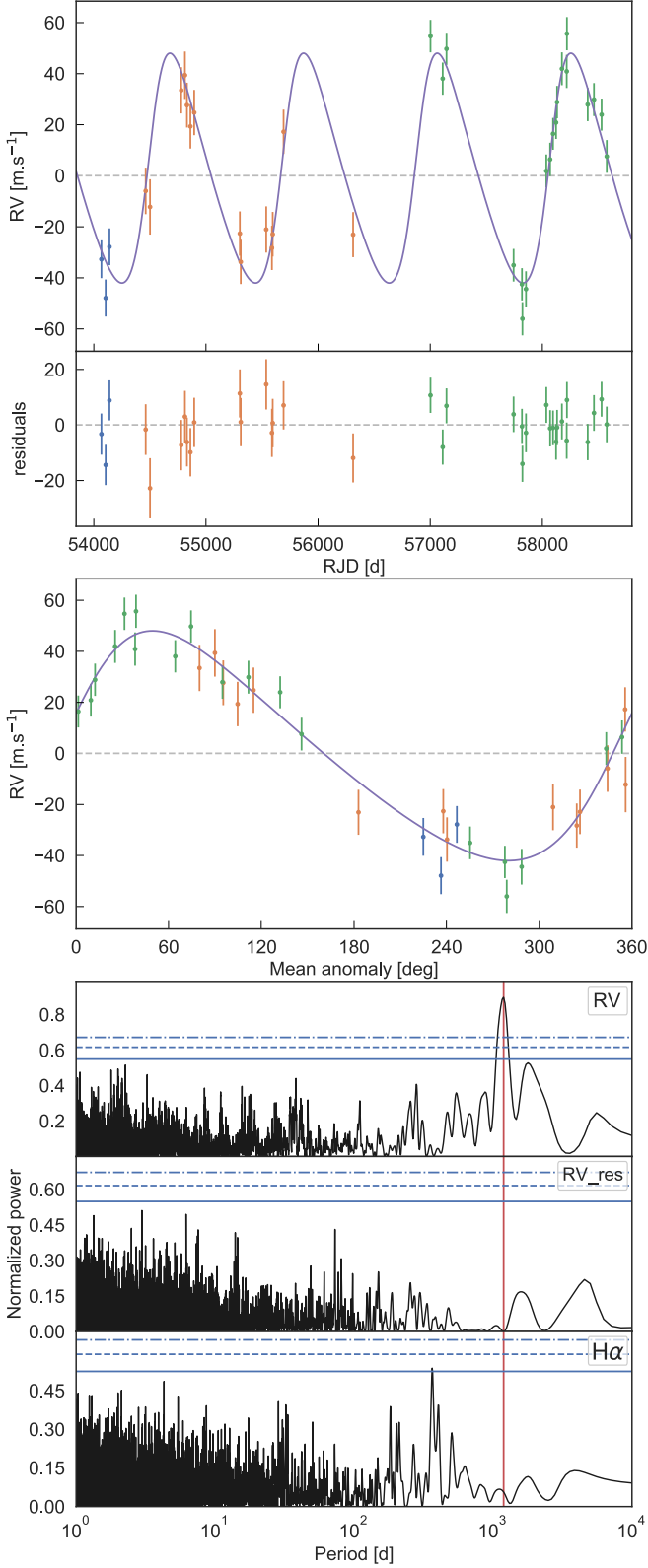


**Fig. 11.** Same as Fig. 9, but for HD 69123. The period of the best solution is 1193.3 days.

### 5.2. HD 64121

In the case of HD 64121<sup>14</sup>, a  $\sim 623$  day periodic variation is fit by a Keplerian model. It corresponds to a planet in a low-

<sup>14</sup> TIC 264770836 ; GAIA DR2 5488303966125344512

eccentricity orbit, 1.5 au away from its star, with a semi-amplitude of  $\sim 55 \text{ m s}^{-1}$  and corresponding to a minimum mass of  $2.6 M_J$  ( $M_\star = 1.18 M_\odot$ ). The periodogram of the radial-velocity residuals, after subtraction of the fit, presents a non-significant peak at  $\sim 1000$  days at the same level as the higher-frequency noise. HD 64121 also exhibits a similar non-significant peak in the periodogram of the  $H\alpha$  activity index (see bottom periodogram in Fig. 10), at  $\sim 550$  days. The weighted Pearson correlation coefficient with the radial-velocities was found to be non-significant at  $R_p = 0.072 \pm 0.116$ . We also computed the weighted Spearman's rank  $R_s = 0.100 \pm 0.118$ , which is also non-significant. We reach the same conclusion as for HD 22532, that those variations are most likely not at the origin of - nor are they linked to - the radial-velocity signal.

### 5.3. HD 69123

Finally, HD 69123<sup>15</sup> presents the longest periodic variation, with a  $\sim 1193$  day signal corresponding to a planet in a slightly eccentric orbit of  $e = 0.2$ . The semi-major axis of the planetary orbit is  $\sim 2.5$  au, and the semi-amplitude  $\sim 47 \text{ m s}^{-1}$  leads to a minimum mass of  $3 M_J$  for the planetary companion ( $M_\star = 1.43 M_\odot$ ). HD 69123 presents a peak in the periodogram of the  $H\alpha$  activity index, with a FAP level below 1% (bottom panel in Fig. 11), at a period of  $\sim 367$  days. We suspect this almost one-year periodicity to be caused by a telluric contamination of the  $H\alpha$  line, and potentially water lines.

### 5.4. Intrinsic variability and final solutions

For the three stars, none of our other activity indicators (contrast, FWHM and BIS) show any similar periodicity or significant correlation with the radial velocities (see Appendix C).

We also checked the V-band photometric data available in the All-Sky Automated Survey (ASAS-3, [Pojmański \(2002\)](#)) for our stars. This survey is very interesting as it is one of the only surveys with a time span of almost nine years. For reasons of consistency and reliability of the data post-processing (mainly correction of saturation and camera focus stability due to instrumental issues), we have to consider this data with caution when using it to check for variability due to intrinsic stellar processes or surface rotational modulation. We discuss this matter in more detail in [Pezzotti et al. \(2021\)](#). No periodicities linked to the ones detected in the radial-velocity data have been found for any of the three stars presented in this paper.

We are thus fairly confident that the observed radial-velocity periodic variations are not due to chromospheric stellar activity, or rotational modulation of surface features such as spots, which would require a significant percentage of the stellar surface to be covered. We also found no indication of long-period, non-radial oscillation modes (neither matching periodicities nor corresponding harmonics in the line profile moments). We thus consider that the observed radial-velocity signals are due to planetary companions orbiting the stars. The resulting models and residuals are shown in Figs. 9–11, overplotted on the radial-velocities. In Table 4, we present the statistics of the distributions (i.e., the median and standard deviation) of the more common set of Keplerian parameters  $P$ ,  $K$ ,  $e$ ,  $\omega$  and  $T_p$ , as well as the distributions of the semi-major axis and minimum masses, derived from the MCMC chains of the fit parameters. In Appendix B, we present the corner plots of the posterior distributions of the fit parameters for each star. The weighted rms scatter of the radial velocities  $rms_{tot}$  and

<sup>15</sup> TIC 146264536; GAIA DR2 5544699390684005248.

**Table 4.** Radial-velocity observation statistics, best-fit solutions of the model with instrumental offsets, nuisance parameters, Keplerian orbital parameters, and inferred planetary parameters.

		HD 22532b	HD 64121b	HD 69123b
<b>Observations</b>				
$N_{obs}$		52	36	36
$T_{span}$	[days]	5016	4853	4507
$rms_{tot}$	[ $m.s^{-1}$ ]	31.15	44.93	31.68
$rms_{res}$	[ $m.s^{-1}$ ]	8.44	15.93	8.42
$\chi^2_{red}$		1.30	1.44	1.69
<b>Offsets <sup>(1)</sup></b>				
$\Delta RV_{COR98-COR07}$	[ $m/s$ ]	$2.0 \pm 2.3$	$-0.1 \pm 3.7$	$-4.1 \pm 3.5$
$\Delta RV_{COR07-COR07}$	[ $m/s$ ]	$29248.9 \pm 1.5$	$-4117.9 \pm 4.0$	$27476.7 \pm 2.4$
$\Delta RV_{COR14-COR07}$	[ $m/s$ ]	$20.9 \pm 2.2$	$15.1 \pm 3.4$	$21.9 \pm 2.8$
<b>Instrumental Noises</b>				
$\sigma_{COR98}$	[ $m/s$ ]	$4.7 \pm 1.0$	$4.9 \pm 1.0$	$5.2 \pm 1.0$
$\sigma_{COR07}$	[ $m/s$ ]	$6.8 \pm 1.2$	$7.8 \pm 1.5$	$7.8 \pm 1.4$
$\sigma_{COR14}$	[ $m/s$ ]	$3.1 \pm 0.5$	$3.0 \pm 0.5$	$3.0 \pm 0.5$
<b>Stellar Jitter</b>				
$\sigma_{jit}$	[ $m.s^{-1}$ ]	$2.1 \pm 1.6$	$16.8 \pm 2.6$	$7.2 \pm 1.8$
<b>Keplerians</b>				
$P$	[days]	$872.6 \pm 2.8$	$623.0 \pm 3.4$	$1193.3 \pm 7.0$
$K$	[ $m.s^{-1}$ ]	$40.0 \pm 1.6$	$55.2 \pm 4.1$	$46.8 \pm 2.4$
$e$		$0.03 \pm 0.03$	$0.11 \pm 0.07$	$0.19 \pm 0.06$
$\omega$	[deg]	$169.1 \pm 88.7$	$2.7 \pm 56.0$	$-67.3 \pm 21.7$
$\lambda_0$ <sup>(2)</sup>	[deg]	$110.7 \pm 2.3$	$-77.5 \pm 7.3$	$227.6 \pm 4.5$
$T_p$ <sup>(2)</sup>	[ $rjd$ ]	$5575.0 \pm 221.0$	$5653.0 \pm 130.0$	$5715.7 \pm 64.6$
$a$	[ $au$ ]	$1.900 \pm 0.004$	$1.510 \pm 0.006$	$2.482 \pm 0.010$
$m_2 \sin i$ <sup>(3)</sup>	[ $M_J$ ]	$2.12 \pm 0.09$	$2.56 \pm 0.19$	$3.04 \pm 0.16$

<sup>1</sup> The reference instrument is COR07.<sup>2</sup> The mean longitude is given at  $BJD = 2\,455\,500$  [d], while 2 450 000 has been subtracted from the date of passage through periastron ( $T_p$ ).<sup>3</sup> Using the model-independent mass from seismic inversions (see [Buldgen et al. 2021](#)).

residuals to the Keplerian fit  $rms_{res}$  are also provided in the table. For all three targets, the rms of the residuals are comparable to those of single giant stars with similar  $B - V$  (see [Hekker et al. 2006b](#) Fig. 3).

## 6. Discussion and conclusion

Since 2006, we have been conducting a high-precision radial-velocity survey of a volume-limited sample of 641 giant stars using the CORALIE spectrograph on the 1.2 m Leonard Euler Swiss telescope at La Silla Observatory (Chile). Our goal is to better understand the formation and evolution of planets around stars more massive than the Sun, including the evolutionary stage of stars toward the giant branch, through a statistical study of the properties of the detected planet population. The sample is volume limited, targeting giant stars in the southern hemisphere (declination  $< 25^\circ$ ) inside a 300 pc radius around the Sun. The evolutionary stage of the stars was constrained by magnitude ( $M_V < 2.5$ ) and color ( $0.78 < B - V < 1.06$ ) cut-offs to avoid main-sequence stars and intrinsically variable late-type giants. We derived reliable spectroscopic parameters from CORALIE-14 spectra (following [Santos et al. 2004](#); [Sousa 2014](#); [Alves et al. 2015](#)). Our sample shows a distribution of a metallicity ratio of iron similar to the one of stars in the solar neighborhood, peaking between 0.0 and 0.1 dex, but missing very low and rich metallicity stars. This may be explained by the young age of the giants, compared to their dwarf counterparts, which did not leave them enough time to migrate in the Galaxy [Wang & Zhao](#)

(2013); [Minchev et al. \(2013\)](#). A color cut-off bias could also be part of the explanation for this effect, excluding the low-log-g stars with high metallicity and the high-log-g stars with low metallicity, as discussed in [Mortier et al. \(2013\)](#); [Adibekyan \(2019\)](#). We also obtained stellar masses for the sample with global parameters fitting, using evolutionary tracks from [Pietrinferni et al. \(2004\)](#), using the SPInS software ([Lebreton & Reese 2020](#)). The distribution ranges approximately from 0.75 to  $4 M_\odot$ , with a maximum around  $2 M_\odot$ .

This paper is the first of a series in which we present the first results of the survey, namely the detection and characterization of three new planetary companions orbiting the giant stars HD 22532, HD 64121, and HD 69123, taking advantage of asteroseismic masses, following the methodology of [Buldgen et al. \(2019\)](#), obtained with the TESS data ([Ricker et al. 2014](#)). For each star, we systematically checked for any correlation with chromospheric activity, rotational modulation of surface features, or long-term non-radial pulsations. We also consulted the corresponding ASAS-3 photometry time series ([Pojmański 2002](#)), spanning 6.8 to 7.4 years. No significant periodicities or correlations linked to the radial-velocity signal detected have been found.

The new planets are typical representatives of the known population of planets around giant stars, considering their masses, semi-major axes, and low eccentricities. This is illustrated in Fig. 12 displaying the new detections together with the planet candidates from the literature. Most planets discovered around giant stars have eccentricities below 0.2-0.3 (e.g., [Jones et al.](#)

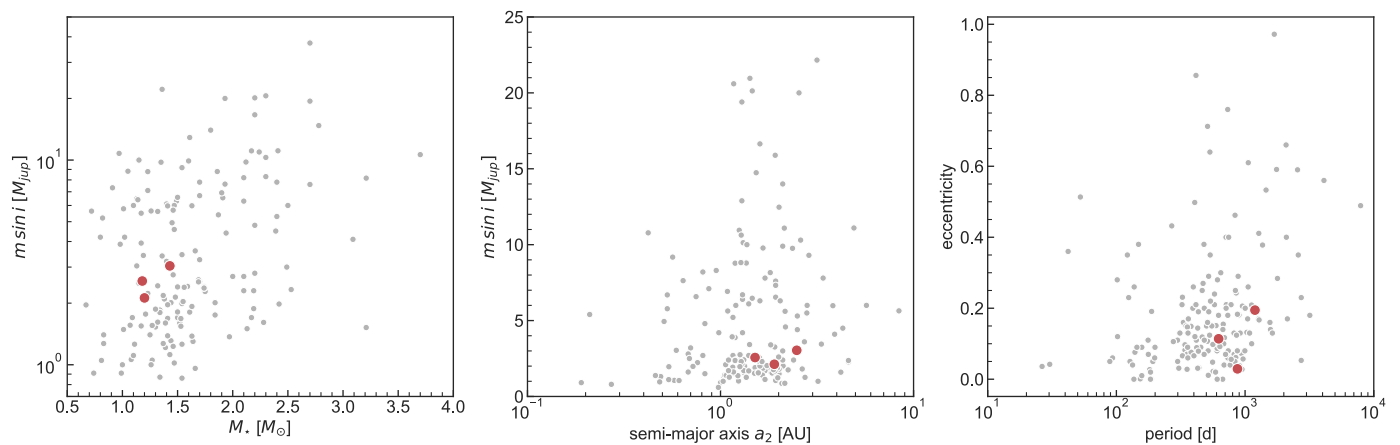


**Fig. 12.** Stellar and planetary parameter relations for the 186 discovered planets orbiting giant stars. The three planets presented in this paper are represented by red dots.

2014; Yilmaz et al. 2017), and are at distances, that is, farther away than 1 au from the central star.

Monitoring of the CASCADES sample is continuing. As an interesting by-product, it is also bringing important information on stellar binaries and star-brown-dwarf systems. The formation scenario for the latter is still unclear. The system may form initially as a binary star with an extreme mass ratio, or through a formation process comparable to the one for planets in the protostellar disk, via disk instability or core accretion. The maximum mass of planets forming in a massive disk is not known. Forthcoming papers will present additional planetary candidates, as well as potential brown dwarfs and spectroscopic binaries found in the sample. We will also address through a statistical study of our sample, the main open questions linked with the planet population orbiting intermediate-mass (evolved) stars: distribution of orbital properties as constraints for planet formation models, correlations between planet characteristics and occurrence rate with primary star properties such as mass and metallicity.

In this context, some planet-host stars from our sample are particularly well suited for a deep asteroseismic analysis, giving access to their internal structure. The available information includes well-constrained planetary signals, long, photometric, high-precision time series from high-cadence observations with TESS, and accurate spectroscopic parameters. Asteroseismologic analysis can provide precious information concerning the past and future evolution of such systems. Among the highly interesting related questions is the one of the impact of stellar evolution on the planet orbits and of the potential engulfment of planets by the star (Pezzotti et al. 2021), for instance to explain the apparent lack of close-in, short-period planets ( $P \leq 100$  days,  $a \leq 0.5$  au). The second and third publications of the CASCADES series will focus on the asteroseismic analysis of the three stellar hosts presented in this paper (Buldgen et al. 2021) and the analysis of a new planet-host star (Pezzotti et al. 2021), for which the full evolution of the system can be modeled.

Giant stars hosting planets are good candidates for planetary transit searches. Due to the increase in radius at the giant stage, companions of giant stars have a higher probability of transit than planets around main-sequence stars. However, as these planets are on long-period orbits, the transit duration is on the order of tens to hundreds of hours. Moreover, because of the relative size of the planet and the star, the expected transit depth is very small. For our sample stars, they are in the 10 – 1000 ppm range. Although very limiting for ground-based observations, these two aspects

are tractable from space with satellites such as TESS (Ricker et al. 2014) and CHEOPS (Benz et al. 2021). The three systems described in this paper present transit probabilities around 1.5 % and transit depth between 170 and 350 ppm (considering planets with a  $1 R_J$  radius). Unfortunately, none of these candidates has thus far had a transit time prediction in the window of the TESS observations.

*Acknowledgements.* We thank all observers at La Silla Observatory from the past fourteen years for their contribution to the observations and the quality of their work. We acknowledge financial support from the Swiss National Science Foundation (SNSF) for the project 2020-178930. This work has, in part, also been carried out within the framework of the National Centre for Competence in Research PlanetS supported by SNSF. In particular, this publication makes use of the The Data & Analysis Center for Exoplanets (DACE, <https://dace.unige.ch>), a platform of Planets, based at the University of Geneva (CH), dedicated to extrasolar planet data visualisation, exchange and analysis. G.B. acknowledges funding from the SNF AMBIZIONE grant No. 185805 (Seismic inversions and modelling of transport processes in stars). P.E. has received funding from the European Research Council (ERC) under the European Union’s Horizon 2020 research and innovation programme (grant agreement No 833925, project STAREX). C.P. acknowledges funding from the Swiss National Science Foundation (project Interacting Stars, number 200020-172505). V. A. acknowledges the support from FCT through Investigador FCT contract no. IF/00650/2015/CP1273/CT0001. N.C.S acknowledges support from FCT - Fundação para a Ciência e a Tecnologia through national funds and by FEDER through COMPETE2020 - Programa Operacional Competitividade e Internacionalização by these grants: UID/FIS/04434/2019; UIDB/04434/2020; UIDP/04434/2020; PTDC/FIS-AST/32113/2017 & POCL-01-0145-FEDER-032113; PTDC/FIS-AST/28953/2017 & POCL-01-0145-FEDER-028953. S.G.S acknowledges the support from FCT through Investigador FCT contract nr. CEECIND/00826/2018 and POPH/FSE (EC). N.L. acknowledges financial support from "Programme National de Physique Stellaire" (PNPS) of CNRS/INSU, France. This research has made use of the NASA Exoplanet Archive, which is operated by the California Institute of Technology, under contract with the National Aeronautics and Space Administration under the Exoplanet Exploration Program.

## References

- Adibekyan, V. Z. 2019, *Geosciences*, 9, 105  
 Adibekyan, V. Z., Benamati, L., Santos, N. C., et al. 2015, *MNRAS*, 450, 1900  
 Aerts, C. & Eyer, L. 2000, in 6th Vienna Work. delta Scuti Relat. Stars, ed. M. Breger & M. Montgomery (Vienna: Astronomical Society of the Pacific), 113  
 Alibert, Y., Mordasini, C., Benz, W., & Winisdoerffer, C. 2005, *A&A*, 434, 343  
 Alonso, A., Arribas, S., & Martínez-Roger, C. 1999, *A&A Suppl. Ser.*, 140, 261  
 Alves, S., Benamati, L., Santos, N. C., et al. 2015, *MNRAS*, 448, 2749  
 Bailer-Jones, C. A. L., Rybizki, J., Fousneau, M., Mantelet, G., & Andrae, R. 2018, *ApJ*, 156, 58  
 Baluev, R. V. 2008, *MNRAS*, 385, 1279

- Baranne, A., Mayor, M., & Poncet, J. 1979, *Vistas Astron.*, 23, 279
- Beck, P. G., Bedding, T. R., Mosser, B., et al. 2011, *Science* (80- ), 332, 205
- Bedding, T. R., Mosser, B., Huber, D., et al. 2011, *Nature*, 471, 608
- Benz, W., Broeg, C., Fortier, A., et al. 2021, *Exp. Astron.*, 51, 109
- Boisse, I., Moutou, C., Vidal-Madjar, A., et al. 2009, *A&A*, 495, 959
- Boss, A. P. 1997, *Science* (80- ), 276, 1836
- Bossini, D., Vallenari, A., Bragaglia, A., et al. 2019, *A&A*, 623, A108
- Briquet, M., Aerts, C., Lüftinger, T., et al. 2004, *A&A*, 413, 273
- Briquet, M., De Cat, P., Aerts, C., & Scuflaire, R. 2001, *A&A*, 380, 177
- Brown, A. G. A., Vallenari, A., Prusti, T., et al. 2018, *A&A*, 616, A1
- Buldrige, G., Ottoni, G., Pezzotti, C., et al. 2021, *A&A*
- Buldrige, G., Rendle, B., Sonoi, T., et al. 2019, *MNRAS*, 482, 2305
- Butler, R. P., Marcy, G. W., Williams, E., Hauser, H., & Shirts, P. 1997, *ApJ*, 474, L115
- Campbell, B., Walker, G. A. H., & Yang, S. 1988, *ApJ*, 331, 902
- Chelli, A. 2000, *A&A*, 358, 59
- da Silva, L., Girardi, L., Pasquini, L., et al. 2006, *A&A*, 458, 609
- De Ridder, J., Barban, C., Baudin, F., et al. 2009, *Nature*, 459, 398
- De Ridder, J., Barban, C., Carrier, F., et al. 2006, *A&A*, 448, 689
- Delgado Mena, E., Lovis, C., Santos, N. C., et al. 2018, *A&A*, 619, A2
- Delisle, J.-B., Hara, N., & Ségransan, D. 2020, *A&A*, 638, A95
- Delisle, J.-B., Ségransan, D., Buchschacher, N., & Alesina, F. 2016, *A&A*, 590, A134
- Delisle, J.-B., Ségransan, D., Dumusque, X., et al. 2018, *A&A*, 614, A133
- Díaz, R. F., Almenara, J.-M., Santerne, A., et al. 2014, *MNRAS*, 441, 983
- Díaz, R. F., Ségransan, D., Udry, S., et al. 2016, *A&A*, 585
- Döllinger, M. P., Hatzes, A. P., Pasquini, L., et al. 2007, *A&A*, 472, 649
- Dumusque, X., Santos, N. C., Udry, S., Lovis, C., & Bonfils, X. 2011, *A&A*, 527, A82
- Dupret, M.-A., Belkacem, K., Samadi, R., et al. 2009, *A&A*, 506, 57
- Durisen, R., Boss, A., Mayer, L., et al. 2007, in *Protostars Planets V*, ed. K. K. B. Reipurth, D. Jewitt (University of Arizona Press), 607–622
- ESA. 1997, *VizieR Online Data Cat.*, ESA SP-120
- Frandsen, S., Carrier, F., Aerts, C., et al. 2002, *A&A*, 394, L5
- Frink, S., Mitchell, D. S., Quirrenbach, A., et al. 2002, *ApJ*, 576, 478
- Frink, S., Quirrenbach, A., Fischer, D. A., Röser, S., & Schilbach, E. 2001, *Publ. Astron. Soc. Pacific*, 113, 173
- Galland, F., Lagrange, A.-M., Udry, S., et al. 2005, *A&A*, 443, 337
- Ghezzi, L., Cunha, K., Schuler, S. C., & Smith, V. V. 2010, *ApJ*, 725, 721
- Girardi, L., Bressan, A., Bertelli, G., & Chiosi, C. 2000, *A&A Suppl. Ser.*, 141, 371
- Gomes da Silva, J., Santos, N. C., Bonfils, X., et al. 2011, *A&A*, 534, A30
- Griffin, R. F. 1967, *ApJ*, 148, 465
- Han, I., Lee, B.-C., Kim, K.-M., et al. 2010, *A&A*, 509, A24
- Hatzes, A. P. & Cochran, W. D. 1993, *ApJ*, 413, 339
- Hatzes, A. P. & Cochran, W. D. 1994, *ApJ*, 422, 366
- Hatzes, A. P. & Cochran, W. D. 1999, *MNRAS*, 304, 109
- Hatzes, A. P., Guenther, E. W., Endl, M., et al. 2005, *A&A*, 437, 743
- Hekker, S. 2006, *Commun. Asteroseismol.*, 147, 121
- Hekker, S. 2007, PhD thesis, Leiden University
- Hekker, S. & Aerts, C. 2010, *A&A*, 515, A43
- Hekker, S., Aerts, C., De Ridder, J., & Carrier, F. 2006a, arXiv [arXiv:0609043]
- Hekker, S., Reffert, S., Quirrenbach, A., et al. 2006b, *A&A*, 454, 943
- Helled, R., Bodenheimer, P., Podolak, M., et al. 2014, in *Protostars Planets VI*, ed. H. Beuther, R. S. Klessen, C. P. Dullemond, & T. Henning (University of Arizona Press), 643–665
- Høg, E., Fabricius, C., Makarov, V. V., et al. 2000, *The Tycho-2 Catalogue of the 2.5 million brightest stars*, Tech. rep., Niels Bohr Institutet
- Izumiura, H. 2005, *J. Korean Astron. Soc.*, 38, 81
- Johnson, J. A., Marcy, G. W., Fischer, D. A., et al. 2006, *ApJ*, 652, 1724
- Jones, M. I., Jenkins, J. S., Bluhm, P., Rojo, P., & Melo, C. H. F. 2014, *A&A*, 566, A113
- Jones, M. I., Jenkins, J. S., Rojo, P., & Melo, C. H. F. 2011, *A&A*, 536, A71
- Lagrange, A.-M., Backman, D. E., & Artymowicz, P. 2000, *Protostars planets IV*, 639
- Lambert, D. L. 1987, *ApJ Suppl. Ser.*, 65, 255
- Larson, A. M., Irwin, A. W., Yang, S. L. S., et al. 1993, *Publ. Astron. Soc. Pacific*, 105, 825
- Lebreton, Y. & Reese, D. R. 2020, *A&A*, 642, A88
- Lee, B.-C., Mkrtychian, D. E., Han, I., Kim, K.-M., & Park, M.-G. 2011, *A&A*, 529, A134
- Lissauer, J. J. 1993, *Annu. Rev. A&A*, 31, 129
- Lovis, C. & Mayor, M. 2007, *A&A*, 472, 657
- Lovis, C. & Udry, S. 2004, in 13th Cambridge Work. Cool Stars. Stellar Syst. Sun
- Luck, R. E. & Heiter, U. 2007, *ApJ*, 133, 2464
- Maldonado, J., Villaver, E., & Eiroa, C. 2013, *A&A*, 554, A84
- Mayor, M. & Queloz, D. 1995, *Nature*, 378, 355
- Minchev, I., Chiappini, C., & Martig, M. 2013, *A&A*, 558, A9
- Mortier, A., Santos, N. C., Sousa, S. G., et al. 2013, *A&A*, 557, A70
- Niedzielski, A., Konacki, M., Wolszczan, A., et al. 2007, *ApJ*, 669, 1354
- Niedzielski, A., Villaver, E., Wolszczan, A., et al. 2015, *A&A*, 573, A36
- Pasquini, L., Brucalassi, A., Ruiz, M. T., et al. 2012, *A&A*, 545, A139
- Pezzotti, C., Ottoni, G., Buldrige, G., et al. 2021, *A&A*
- Pietrinfermi, A., Cassisi, S., Salaris, M., & Castelli, F. 2004, *ApJ*, 612, 168
- Pojmański, G. 2002, *Acta Astron.*, 52, 397
- Pollack, J. B., Hubickyj, O., Bodenheimer, P., et al. 1996, *Icarus*, 124, 62
- Queloz, D., Henry, G. W., Sivan, J. P., et al. 2001, *A&A*, 379, 279
- Queloz, D., Mayor, M., Weber, L., et al. 2000, *A&A*, 354, 99
- Quirrenbach, A., Reffert, S., & Bergmann, C. 2011, in *Planet. Syst. BEYOND MAIN Seq.*, ed. S. Schuh, H. Drechsel, & U. Heber, Vol. 102 (Bamberg: AIP), 102–109
- Raymond, S. N., Kokubo, E., Morbidelli, A., Morishima, R., & Walsh, K. J. 2014, in *Protostars Planets VI*, ed. H. Beuther, R. S. Klessen, C. P. Dullemond, & T. Henning (University of Arizona Press), 595–618
- Ribas, A., Bouy, H., & Merín, B. 2015, *A&A*, 576, A52
- Ricker, G. R., Winn, J. N., Vanderspek, R., et al. 2014, in *Sp. Telesc. Instrum. 2014 Opt. Infrared, Millim. Wave*, ed. J. M. Oschmann, M. Clampin, G. G. Fazio, & H. A. MacEwen, Vol. 9143 (SPIE), 914320
- Santos, N. C., Gomes da Silva, J., Lovis, C., & Melo, C. H. F. 2010, *A&A*, 511
- Santos, N. C., Israelian, G., & Mayor, M. 2001, *A&A*, 373, 1019
- Santos, N. C., Israelian, G., & Mayor, M. 2004, *A&A*, 415, 1153
- Santos, N. C., Mortier, A., Faria, J. P., et al. 2014, *A&A*, 566, A35
- Sato, B., Izumiura, H., Toyota, E., et al. 2007, *ApJ*, 661, 527
- Sato, B., Kambe, E., Takeda, Y., et al. 2005, *Publ. Astron. Soc. Japan*, 57, 97
- Ségransan, D., Delisle, J.-B., & Dumusque, X. 2021, *A&A*, submitted
- Ségransan, D., Udry, S., Mayor, M., et al. 2010, *A&A*, 511, A45
- Setiawan, J., Pasquini, L., da Silva, L., von der Lühe, O., & Hatzes, A. P. 2003, *A&A*, 397, 1151
- Snedden, C. A. 1973, PhD thesis, University of Texas
- Sousa, S. G. 2014, in *Determ. Atmos. Parameters B-, A-, F- G-Type Stars*, ed. B. S. Ewa Niemczura & W. Pych (Springer International Publishing), 297–310
- Sousa, S. G., Santos, N. C., Adibekyan, V. Z., Delgado Mena, E., & Israelian, G. 2015, *A&A*, 577, A67
- Sousa, S. G., Santos, N. C., Israelian, G., Mayor, M., & Monteiro, M. J. P. F. G. 2007, *A&A*, 469, 783
- Sousa, S. G., Santos, N. C., Mayor, M., et al. 2008, *A&A*, 487, 373
- Takeda, Y., Sato, B., & Murata, D. 2008, *Publ. Astron. Soc. Japan*, 60, 781
- Tsantaki, M., Sousa, S. G., Adibekyan, V. Z., et al. 2013, *A&A*, 555, A150
- Udry, S., Mayor, M., Maurice, E., et al. 1999, *Int. Astron. Union Colloq.*, 170, 383
- Udry, S., Mayor, M., Naef, D., et al. 2000, *A&A*, 356, 590
- Udry, S. & Santos, N. C. 2007, *Annu. Rev. A&A*, 45, 397
- Walker, G. A. H., Yang, S., Campbell, B., & Irwin, A. W. 1989, *ApJ*, 343, L21
- Wang, Y. & Zhao, G. 2013, *ApJ*, 769, 4
- Wilson, O. C. 1978, *ApJ*, 226, 379
- Winn, J. N. & Fabrycky, D. C. 2014, *Annu. Rev. Astron. Astrophys*
- Wittenmyer, R. A., Endl, M., Wang, L., et al. 2011, *ApJ*, 743, 184
- Yilmaz, M., Sato, B., Bikmaev, I., et al. 2017, *A&A*, 608, A14

**Appendix A: Online material - Radial-velocity data****Table A.2.** Radial-velocity measurements and uncertainties for HD 64121 obtained with the CORALIE spectrograph.**Table A.1.** Radial-velocity measurements and uncertainties for HD 22532 obtained with the CORALIE spectrograph.

JD-2 400 000	RV [ $m s^{-1}$ ]	e_RV [ $m s^{-1}$ ]	Instrument
53469.478311	29290.32	5.11	CORALIE98
53469.489712	29288.82	4.74	CORALIE98
53644.880135	29275.72	3.38	CORALIE98
53721.640656	29246.08	4.06	CORALIE98
53740.549274	29241.64	3.52	CORALIE98
53740.560662	29236.16	3.25	CORALIE98
53967.913052	29207.90	4.05	CORALIE98
54104.541987	29245.90	4.31	CORALIE98
54104.553387	29243.63	4.70	CORALIE98
54472.657418	29283.05	4.61	CORALIE07
54682.939662	29208.02	3.93	CORALIE07
54734.882351	29213.52	6.86	CORALIE07
54772.782614	29206.07	5.79	CORALIE07
54777.726842	29200.32	5.71	CORALIE07
54827.668046	29215.82	3.52	CORALIE07
54861.626764	29207.45	4.26	CORALIE07
54889.547083	29218.61	4.95	CORALIE07
55104.768278	29267.47	3.49	CORALIE07
55166.737312	29278.42	3.31	CORALIE07
55257.569019	29290.95	6.97	CORALIE07
55292.519484	29278.81	3.76	CORALIE07
55310.462662	29280.85	4.70	CORALIE07
55383.942691	29258.97	4.50	CORALIE07
55397.859121	29267.41	4.65	CORALIE07
55414.898447	29243.86	4.30	CORALIE07
55439.891366	29256.90	3.76	CORALIE07
55488.839456	29232.54	3.61	CORALIE07
55546.594910	29220.18	4.09	CORALIE07
55565.675911	29226.35	3.99	CORALIE07
55568.618415	29218.36	4.09	CORALIE07
55578.535688	29211.46	4.04	CORALIE07
55587.635405	29226.81	5.37	CORALIE07
55852.849665	29227.43	4.86	CORALIE07
55871.644660	29241.42	4.03	CORALIE07
56188.802495	29288.00	16.42	CORALIE07
56244.610195	29285.39	11.70	CORALIE07
56281.658388	29271.27	7.84	CORALIE07
56643.747865	29219.51	2.73	CORALIE07
56944.861399	29295.30	2.63	CORALIE07
56989.533778	29334.76	13.20	CORALIE14
57323.731544	29237.66	2.97	CORALIE14
57672.841328	29281.02	5.27	CORALIE14
57733.669500	29300.58	2.59	CORALIE14
57806.516799	29310.84	6.31	CORALIE14
57823.510176	29294.34	5.93	CORALIE14
58004.841570	29269.43	7.14	CORALIE14
58068.689478	29278.41	4.27	CORALIE14
58069.754285	29271.81	4.60	CORALIE14
58122.674719	29259.59	6.61	CORALIE14
58315.907826	29236.10	6.68	CORALIE14
58366.842150	29239.08	7.75	CORALIE14
58485.581907	29271.44	6.19	CORALIE14

We note that small radial-velocity offsets between each instruments have to be considered. The offsets between COR98 and COR07 and between COR14 and COR07 are considered as free parameters in the model (see Table 4).

JD-2 400 000	RV [ $m s^{-1}$ ]	e_RV [ $m s^{-1}$ ]	Instrument
53720.804034	-4060.69	2.91	CORALIE98
53778.680612	-4061.51	2.56	CORALIE98
53803.605854	-4063.90	2.76	CORALIE98
54498.738216	-4115.92	5.18	CORALIE07
54778.828477	-4149.64	6.10	CORALIE07
54811.805888	-4138.88	5.41	CORALIE07
54889.595806	-4118.86	4.85	CORALIE07
54894.556246	-4113.83	3.58	CORALIE07
55302.504568	-4154.21	4.40	CORALIE07
55303.624298	-4177.41	4.61	CORALIE07
55579.781780	-4083.50	3.20	CORALIE07
55673.598495	-4059.93	4.68	CORALIE07
56292.793971	-4039.50	6.72	CORALIE07
56993.853501	-4092.41	4.82	CORALIE14
57147.557314	-4115.81	3.22	CORALIE14
57369.806710	-4073.18	2.93	CORALIE14
57414.644584	-4081.40	5.05	CORALIE14
57496.490076	-4079.47	3.37	CORALIE14
57683.819281	-4148.65	5.41	CORALIE14
57732.846915	-4160.13	3.66	CORALIE14
57808.614926	-4154.18	4.96	CORALIE14
57887.545841	-4149.76	4.23	CORALIE14
58003.902541	-4086.34	6.80	CORALIE14
58034.854274	-4059.25	6.03	CORALIE14
58068.819513	-4036.22	3.90	CORALIE14
58071.860251	-4038.67	3.90	CORALIE14
58121.684266	-4035.53	4.36	CORALIE14
58125.767030	-4042.36	3.95	CORALIE14
58129.671706	-4045.81	4.37	CORALIE14
58173.764097	-4041.42	4.82	CORALIE14
58220.512518	-4054.95	4.19	CORALIE14
58366.910528	-4120.28	7.19	CORALIE14
58406.853503	-4151.65	4.67	CORALIE14
58459.644905	-4155.20	3.85	CORALIE14
58527.581933	-4128.58	3.14	CORALIE14
58573.499140	-4153.03	6.36	CORALIE14

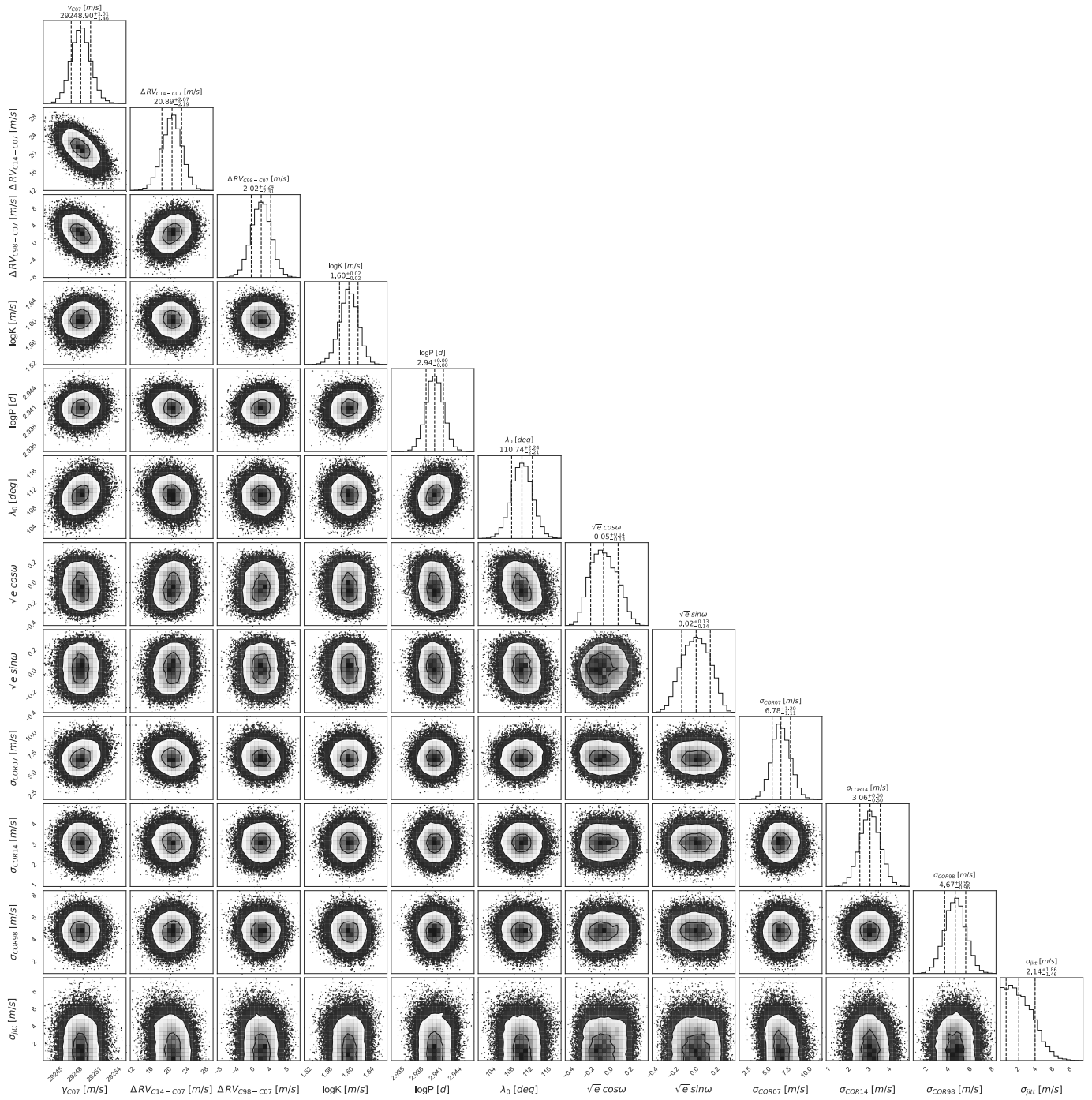
Same as Table A.1.

**Table A.3.** Radial-velocity measurements and uncertainties for HD 69123 obtained with the CORALIE spectrograph.

JD-2 400 000	RV [ $m s^{-1}$ ]	e_RV [ $m s^{-1}$ ]	Instrument
54066.795409	27431.94	2.21	CORALIE98
54104.739993	27416.74	1.63	CORALIE98
54138.713749	27436.81	1.42	CORALIE98
54461.826098	27471.03	3.81	CORALIE07
54500.653028	27464.76	6.99	CORALIE07
54778.840694	27510.46	3.66	CORALIE07
54811.830340	27516.37	4.22	CORALIE07
54829.726766	27504.65	2.92	CORALIE07
54860.593499	27496.33	2.65	CORALIE07
54894.597395	27501.75	3.19	CORALIE07
55301.540504	27454.35	2.54	CORALIE07
55309.605268	27443.25	2.62	CORALIE07
55536.858310	27455.94	3.65	CORALIE07
55587.747458	27448.72	2.54	CORALIE07
55594.692659	27454.08	2.76	CORALIE07
55691.556206	27494.23	2.62	CORALIE07
56311.717839	27453.93	3.06	CORALIE07
57001.851834	27555.54	2.52	CORALIE14
57110.683730	27538.88	2.44	CORALIE14
57144.565060	27550.56	2.37	CORALIE14
57742.816909	27465.79	2.65	CORALIE14
57817.519883	27458.31	2.45	CORALIE14
57821.536651	27444.81	2.90	CORALIE14
57853.479450	27456.43	3.84	CORALIE14
58034.879487	27502.73	2.77	CORALIE14
58068.785220	27507.23	2.95	CORALIE14
58094.717728	27517.27	2.24	CORALIE14
58121.688868	27521.69	2.72	CORALIE14
58130.724735	27529.70	2.48	CORALIE14
58173.733307	27542.76	2.76	CORALIE14
58216.553852	27541.73	2.90	CORALIE14
58218.506427	27556.51	2.87	CORALIE14
58403.872417	27528.76	2.91	CORALIE14
58459.660012	27530.71	2.75	CORALIE14
58527.594463	27524.80	2.32	CORALIE14
58573.495729	27508.41	2.67	CORALIE14

Same as Table A.1.



**Appendix B: MCMC - corner plots distributions of fit parameters**


**Fig. B.1.** Posterior distributions of fit parameters of HD22532. Each panel contains the two-dimensional histograms of the 1 200 000 samples (after removal of the burn-in, the first 25% of the chains). Contours are drawn to improve the visualization of the  $1\sigma$  and  $2\sigma$  confidence interval levels. The upper panels of the corner plot show the probability density distributions of each orbital parameter of the final MCMC sample. The vertical dashed lines mark the 16th, 50th, and 84th percentiles of the overall MCMC samples, delimiting the  $1\sigma$  confidence interval.

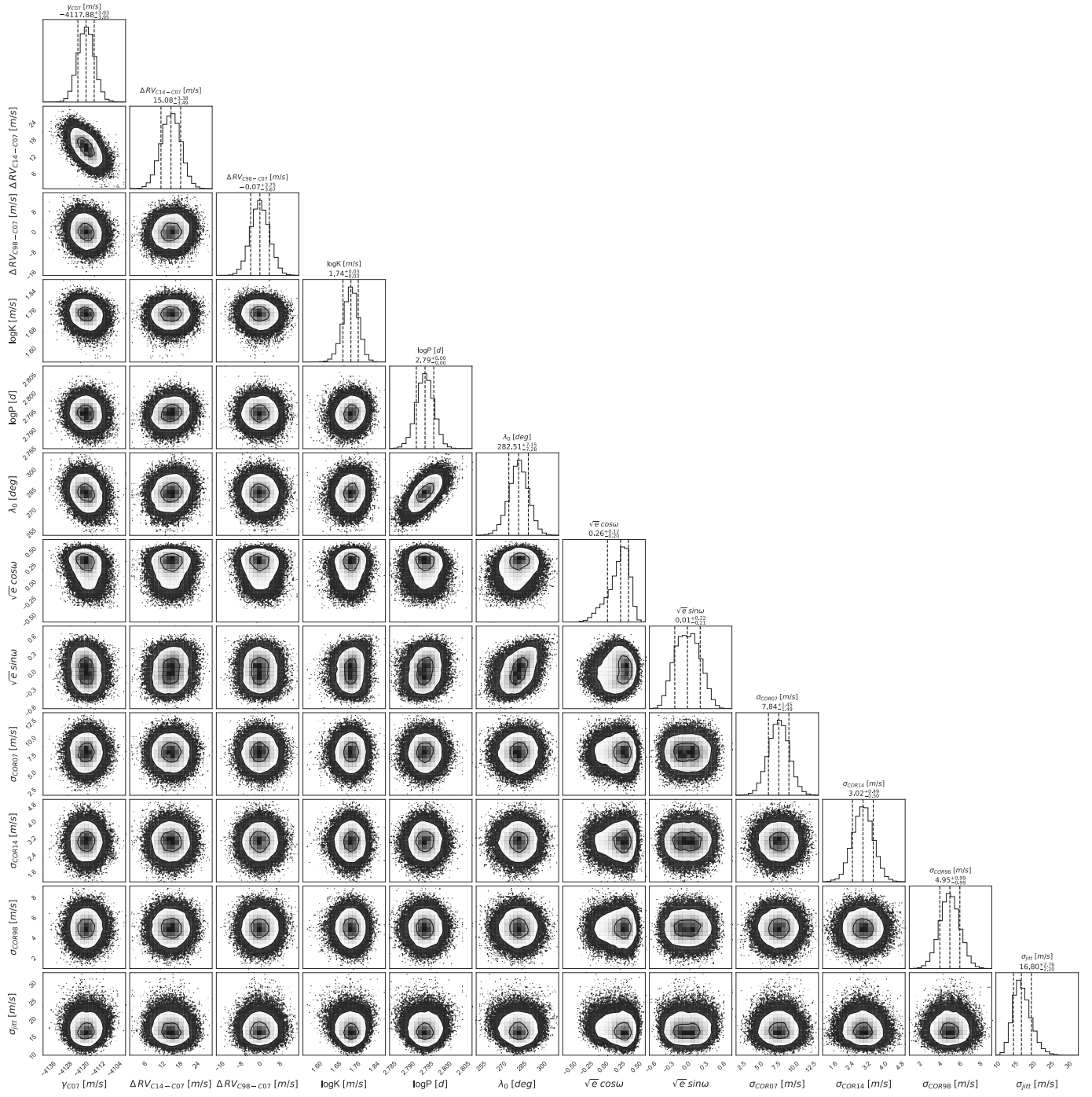


**Fig. B.2.** Same as Fig. A, but for HD 64121.

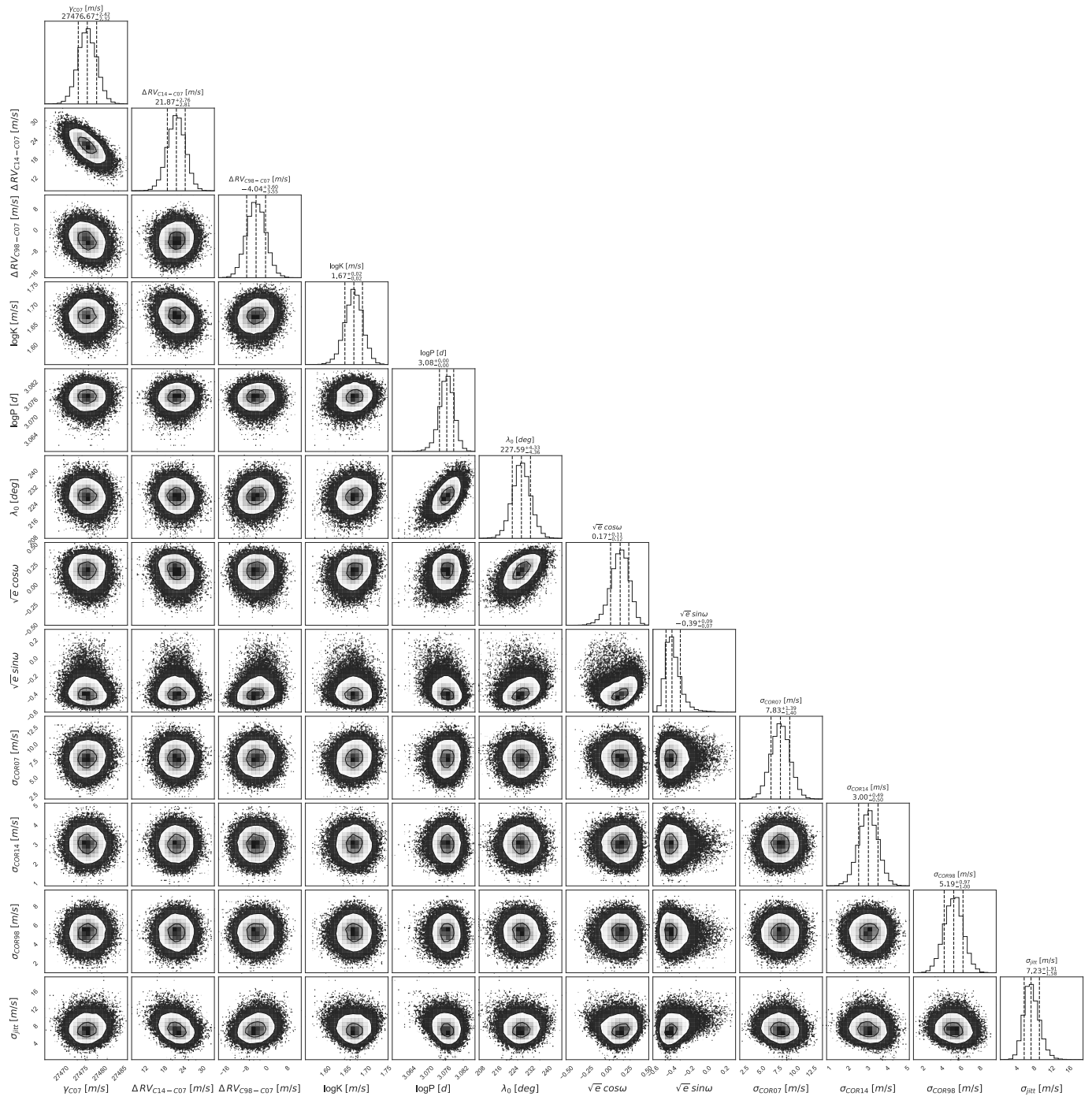
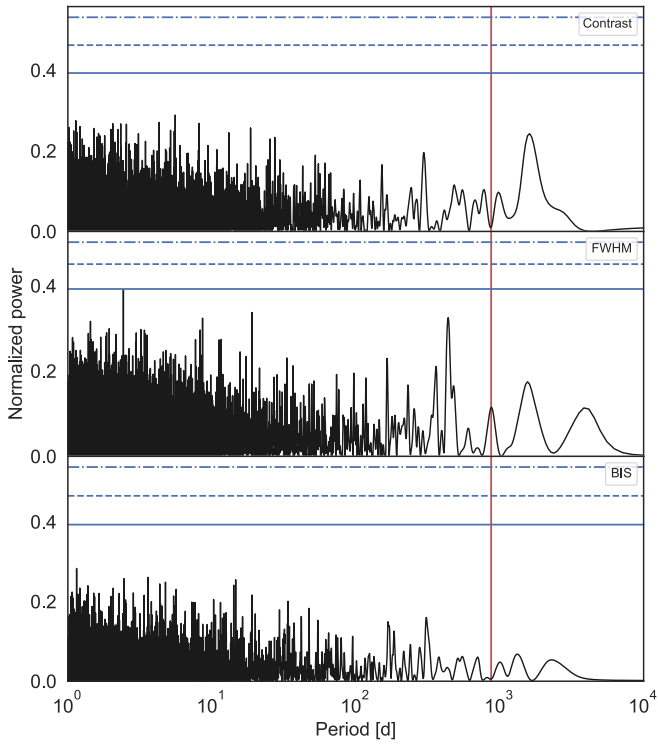
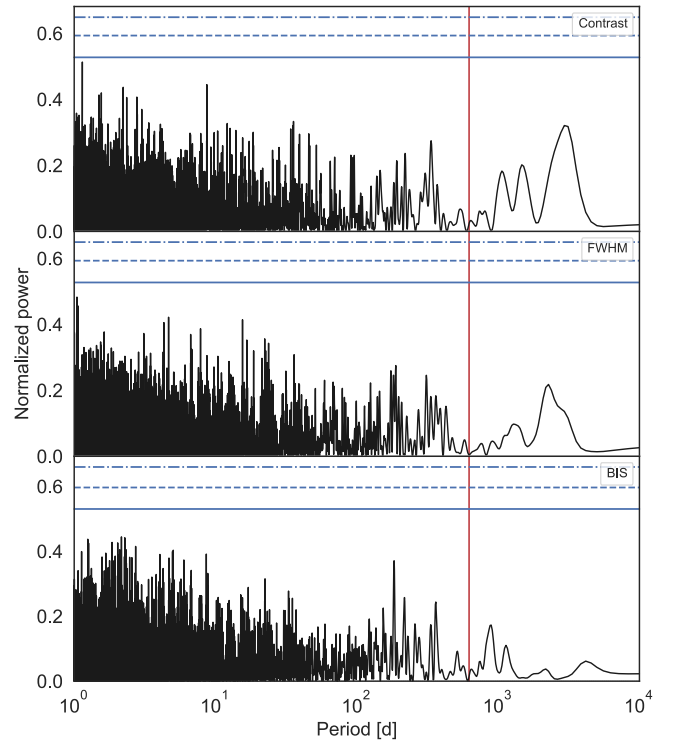


Fig. B.3. Same as Fig. A, but for HD 69123.

### Appendix C: Intrinsic variability analysis - periodograms of line profile indicators



**Fig. C.1.** Periodogram of full width at half maximum (first panel), Bisector inverse span (second panel), and contrast (third panel) for HD22532. The red vertical line represents the fit period in the radial velocity at 872.6 days. Horizontal lines, from bottom to top, are the FAP levels at 10%, 1%, and 0.1%, respectively.



**Fig. C.2.** Same as Fig. C.1, but for HD 64121. The period of the best solution is 623.0 days.

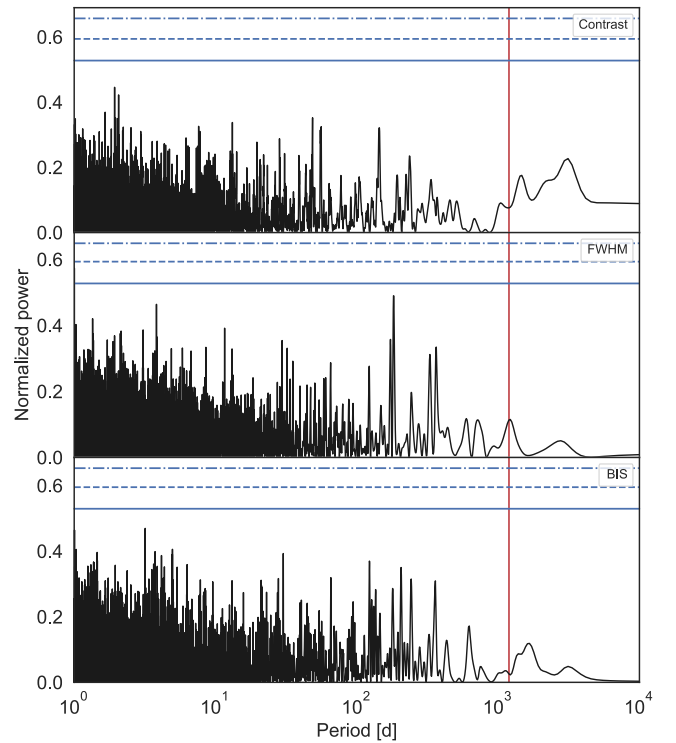


**Fig. C.3.** Same as Fig. C.1, but for HD 69123. The period of the best solution is 1193.3 days.